Design of Hydrogen Solid Oxide Fuel Cells in Blended-Wing–Body Aircraft

Oi Ching Vanessa Chung,* Khaled AlSamri,† Jacqueline Huynh,‡ and Jack Brouwer§
University of California, Irvine, Irvine, California 92697

https://doi.org/10.2514/1.C038174

This paper presents the design methodology for integrating a hydrogen solid oxide fuel cell/gas turbine (SOFC/GT) propulsion system into a blended-wing–body (BWB) aircraft and tube-and-wing (T&W) configurations for 365 and 162 passengers. The design methodology utilizes aircraft sizing and modeling tools that encompass aerodynamic properties, structural design, and powertrain integration. The proposed hydrogen BWB and T&W aircraft are compared against conventional models like the B777-300ER and B737-800. Key results indicate significant reductions in fuel consumption and emissions. For instance, the hydrogen BWB aircraft, on average, exhibits a 56% reduction in Megajoule of fuel energy consumption per passenger-kilometer compared to conventional aircraft. The analysis highlights the environmental benefits, with CO_2 equivalent emissions per passenger-kilometer being significantly lower for hydrogen-powered models. The total takeoff weight per passenger for the hydrogen BWB-365 is 714 kg, compared to 916 kg for the conventional B777-300ER. Hydrogen aircraft configurations, on average, also show a 21% increase and 99.48% decrease in H_2O and NO_x emissions. Moreover, hydrogen BWB configurations exhibit reduced emissions compared to hydrogen T&W despite higher takeoff weights. This study underscores the potential of hydrogen SOFC/GT systems and BWB configurations to enhance efficiency and reduce the environmental impacts for future aircraft.

Nomenclature

A	=	area
a_{takeoff}	=	takeoff acceleration, m/s^2
AOA	=	angle of attack
AR	=	aspect ratio
C_p	=	specific heat at constant pressure, $\text{J/(kg} \cdot \text{K)}$
D_{NAC}	=	nacelle diameter, m
D_{total}	=	total drag, N
F_{THRUST}	=	thrust force, N
h	=	heat transfer coefficient, $\text{W/(m}^2 \cdot \text{K)}$
L	=	characteristic length, m
L/D	=	lift-to-drag ratio, or aerodynamic efficiency
LHV	=	lower heating value, J/kg
Ma	=	Mach number
mac	=	mean aerodynamic chord, m
MTOW	=	maximum takeoff weight
$\dot{m}_{\text{air,compressor}}$	=	air entering the compressor, kg/s
$\dot{m}_{\text{air,fuelheater}}$	=	air entering the fuel heater, kg/s
$\dot{m}_{\text{air,SOFC}}$	=	air entering the solid oxide fuel cell, kg/s
$\dot{m}_{\text{combustor}}$	=	combined flow entering the combustor (from solid oxide fuel cell and fuel), kg/s
$\dot{m}_{\text{exhaust}}$	=	exhaust flow from turbines, kg/s
$\dot{m}_{\text{fuel,combustor}}$	=	fuel flow directly to the combustor, kg/s
$\dot{m}_{\text{fuel,pump}}$	=	fuel flow toward the fuel pump, kg/s
$\dot{m}_{\text{loss}}$	=	heat loss from the fuel heater, W
$\dot{m}_{\text{steam}}$	=	steam flow toward the solid oxide fuel cell, kg/s
$\dot{m}_{\text{turbines}}$	=	flow from combustor to turbines, kg/s
Nu	=	Nusselt number
n_{GH_2}	=	moles of gaseous hydrogen, mol
OEW	=	operating empty weight
P	=	pressure, Pa
Pr	=	Prandtl number
$P_{\text{saturation,ice}}$	=	saturation pressure of ice, Pa
$P_{\text{saturation,water}}$	=	saturation pressure of water, Pa
$Q_{\text{conduction}}$	=	heat transfer due to conduction, W
$Q_{\text{convection}}$	=	heat transfer due to convection, W
$Q_{\text{radiation}}$	=	heat transfer due to radiation, W
Q_{total}	=	total heat transfer, W
R	=	thermal resistance, Ω
R_{gas}	=	gas constant, $\text{J/(mol} \cdot \text{K)}$
Re	=	Reynolds number
T_{NAC}	=	nacelle constant
T_{air}	=	air temperature, K
T_{surface}	=	surface temperature, K
TOFL	=	takeoff field length, m
t/c	=	thickness-to-chord ratio
U_{gas}	=	internal energy of gas, J
V_{takeoff}	=	takeoff velocity, m/s
W_{empty}	=	aircraft empty weight, kg
W_{fuel}	=	fuel weight, kg
W_{NAC}	=	nacelle weight, kg
$W_{\text{op. items}}$	=	operating items weight, kg
W_{payload}	=	payload weight, kg
$W_{\text{propulsion}}$	=	propulsion weight, kg
$W_{\text{structure}}$	=	airframe structure weight, kg
W_{systems}	=	systems and equipment weight, kg
X_{NAC}	=	nacelle length, m
ZFW	=	zero fuel weight, kg
γ	=	climb/descent angle, rad
$\epsilon_{\text{H}_2\text{O}}$	=	emissivity of water
η	=	efficiency
μ	=	dynamic viscosity, $\text{Pa} \cdot \text{s}$
ρ	=	density, kg/m^3

Presented as Paper 2024-3664 at the AIAA Aviation 2024 Forum, Las Vegas, NV, July 29, 2024; received 8 August 2024; accepted for publication 3 December 2024; published online 7 February 2025.

*Graduate Student, Department of Mechanical and Aerospace Engineering, 4200 Engineering Gateway; occhung@uci.edu. Student Member AIAA (Corresponding Author).

†Graduate Student, Department of Mechanical and Aerospace Engineering, 4200 Engineering Gateway; kalsamri@uci.edu. Student Member AIAA.

‡Assistant Professor, Department of Mechanical and Aerospace Engineering, 4200 Engineering Gateway; huynhlj@uci.edu. Member AIAA.

§Director of Advanced Power and Energy Program, Department of Mechanical and Aerospace Engineering, 4200 Engineering Gateway; jb@nfcrc.uci.edu. Member AIAA.

I. Introduction

EVIDENCE has shown that the aviation industry contributed roughly 920 million tons of carbon dioxide emissions in 2019, and this figure is anticipated to rise in the future [1]. Notably, the United

States, boasting the largest commercial air traffic system globally, accounted for about 23% of these emissions in 2017 [1]. Furthermore, research has revealed that the combustion of aviation fuel during various flight procedures releases harmful ultrafine particles, linked to health problems such as respiratory system damages and potential lung cancer [2]. Additionally, the research indicated that the magnitude of emissions is correlated with aircraft size, as exemplified by the Boeing 767-400ER and Boeing 787 in the 200,000 kg weight category, emitting an average peak concentration of 26,500 particles in each cubic centimeter of air [2]. Additionally, nitrogen oxide (NOx) emissions from aircraft engines, particularly during high-temperature combustion processes, further exacerbate air pollution and climate change. NOx emissions contribute significantly to the formation of ground-level ozone and smog, posing additional environmental and health risks, and have been shown to adversely affect local air quality and public health in areas surrounding major airports [2]. Consequently, transitioning to sustainable aviation through aircraft electrification holds promise for mitigating industry-related emissions.

The subject of sustainable aviation encompasses a diverse range of considerations, spanning the optimization of aircraft configurations, the electrification of aircraft propulsion systems, and the examination of flight procedures to best mitigate noise propagation, among other facets. Reducing aircraft criteria pollutant and greenhouse gas (GHG) emissions demands particular attention within the field of aerospace engineering, driven by the current environmental impact associated with emissions from the aviation industry. One of the proposed solutions to promote a greener aviation environment is the integration of fuel cell and battery technologies into existing propulsion systems. Several prior publications have explored the possibilities of integrating diverse electric propulsion systems into existing aircraft configurations. The study by Valencia et al. investigated a hydrogen-powered hybrid solid oxide fuel cell/gas turbine (SOFC/GT) within a turboelectric distributed propulsion based on the NASA N3-X blended-wing–body (BWB) planform [3,4]. It reveals that this configuration, when using liquid hydrogen, can potentially reduce thrust specific fuel consumption (TSFC) by 70%. However, it also identifies significant challenges, such as hydrogen storage issues and a 40% increase in propulsion system weight due to the incorporation of fuel cells [3]. Moreover, the study by Adler and Martins assesses hydrogen-powered aircraft's potential for greater climate impact reductions at lower costs compared to biofuels [5]. Despite hydrogen's higher storage volume, the BWB configuration is seen as efficient for large fuel tanks. Comparing optimized kerosene and hydrogen versions of BWB and tube-and-wing (T&W) aircraft, the study finds that a hydrogen BWB has a 3.8% energy penalty compared to its kerosene counterpart, while the T&W hydrogen design has a 5.1% penalty compared to its kerosene counterpart. This advantage diminishes without lightweight hydrogen tanks. Any kerosene BWB fuel efficiency benefits also apply to hydrogen versions, highlighting the value of advancing kerosene BWB technology for future hydrogen aircraft [5].

The prevailing configuration for contemporary passenger airliners is characterized by a T&W design, featuring dual engines mounted underneath the wings and a conventional empennage configuration. Historically, blended-wing–bodies have primarily found application in fighter jets and bombardiers remained within the realm of experimental exploration. The BWB concept has its roots in efforts to improve aircraft efficiency by reducing aerodynamic drag, structural weight, and enhancing engine performance. The concept gained significant attention in the 1990s, particularly through the work of McDonnell Douglas and NASA. Key developments include the initial BWB-800-I project, followed by the BWB-800-II, which demonstrated the feasibility and potential performance benefits of the BWB design. A significant milestone in the development of the BWB was the BWB-450 project, which aimed to create a more practical and marketable version of the concept. This project involved optimizing the BWB design to balance aerodynamic efficiency, structural integrity, and operational feasibility. The BWB-450 featured a more refined planform with a longer centerbody and new transonic airfoils, resulting in improved aerodynamic performance and stability. It also shows a potential of scaling up or down of the cabin and airframe to accommodate a wide range of passengers and payloads. These advancements and advantages made the BWB-450 a key reference point for subsequent BWB research and development efforts [6,7], including this paper. Moreover, notably, JetZero has recently introduced an innovative BWB design specifically tailored for flight trajectories spanning up to 5000 nautical miles (nmi). The slated official launch of this groundbreaking research initiative is anticipated by the year 2030 [8]. Additionally, several conceptual airplanes, like the Airbus ZEROe, utilize hybrid-hydrogen turbofans and electric propulsion systems [9]. Notably, Airbus proposed a hydrogen BWB concept in 2020. Combining a BWB airframe with a hydrogen fuel cell system remains relatively unexplored [9]. Our goal is to harness BWB efficiency and hydrogen fuel cell propulsion gains, offering a unique opportunity to optimize aircraft performance.

In the pursuit of sustainable aviation, hydrogen-powered BWB aircraft offer notable aerodynamic and storage advantages. The design reduces skin friction drag due to decreased wetted area, minimizes trim drag from relaxed pitch stability, and lowers interference drag through the smooth centerbody-wing transition. The lifting body improves spanwise lift distribution, reducing lift-induced drag and enhancing aerodynamic efficiency. BWB's area-ruled shape lowers wave drag at high transonic speeds, and higher wing loading compared to traditional T&W aircraft increases fuel efficiency at higher cruise speeds. The configuration provides increased internal volume, ideal for hydrogen storage tanks, and superior noise shielding through engine integration. However, tradeoffs include the noncircular pressurized body adding weight, relaxed stability complicating flight control, and the tailless design posing recovery challenges during tumbling. Degraded repairability compared to T&W, limitations with airport taxiway and runway width, and gate size increase complications. Additionally, integrating hydrogen storage without compromising aerodynamic efficiency or center of gravity (CG) is challenging. Safety concerns about hydrogen leakage and fuel cell reliability persist, reflecting the complex balance between innovation and practicality in hydrogen-powered BWB aircraft [6].

Several papers have investigated the hydrogen BWB synergy; Adler and Martins research compares a kerosene versus hydrogen T&W and BWB. The result that a hydrogen-powered BWB aircraft exhibits a mere 3.1% increase in energy consumption compared to its kerosene counterpart, outperforming the hydrogen T&W aircraft's 5.1% increase, introduces the BWB configuration's applicability and efficiency in hydrogen adaptation [5]. Additionally, the paper highlights the feasibility of both hydrogen and BWB designs for aviation [5]. The BWB configurations exhibit higher average cruise lift-to-drag (L/D) ratios (24.8 for kerosene and 23.3 for hydrogen) compared to T&W designs (19.7 for kerosene and 19.4 for hydrogen), indicating superior aerodynamic efficiency. Hydrogen-powered aircraft demonstrate significantly lower maximum takeoff weight (MTOW) and fuel weights, suggesting reduced fuel consumption and environmental impact. However, hydrogen configurations have higher operating empty weights (OEWs), which may mitigate some of these advantages. Notably, the hydrogen BWB has the lowest MTOW, being 18.5 and 13% lighter than the kerosene T&W and hydrogen T&W aircraft designs, respectively. Overall, the BWB design and hydrogen fuel show strong potential for more efficient and sustainable aviation, though challenges remain in managing the higher OEW associated with hydrogen systems. Further, Karpuk et al. shed light on the environmental impacts, illustrating a substantial reduction in CO_2 emissions for hydrogen-powered BWB aircraft by 81% using green hydrogen and an 88% reduction compared to a conventional B777-300ER [10]. Additionally, Kissoon et al. provided valuable insights into the performance capabilities of BWB aircraft with different fuels using a point-mass approach, despite their research focusing on the military sector [11]. Their findings indicate that using kerosene BWB results in a 42% increase in payload over a design range of 7500 nmi against the existing Boeing 777-200LR as a baseline. When using liquid hydrogen, the range is limited to about 3000 nmi due to the low density of the fuel. However, at this reduced range, the payload can be increased by 137%, reaching 127,000 kg [11].

This paper presents the design methodology for integrating a hydrogen SOFC/GT propulsion system into a BWB aircraft, focusing on

fuel cell integration in BWB designs. The study compares various aircraft sizes to understand configuration and sizing tradeoffs, examining the synergy between hydrogen power systems and BWB designs. It also evaluates these configurations against conventional and hydrogen T&W designs to assess performance metrics such as fuel consumption and emissions. The aim is to determine the potential of hydrogen SOFC/GT systems and BWB configurations in enhancing efficiency and reducing the environmental impact of aviation. A multifaceted approach was employed to enhance the outcomes of the project. The utilization of the airframe design and weight model facilitated a comprehensive analysis of aircraft systems, while SolidWorks was instrumental in configuring a visual representation of the proposed designs. The scope of expertise also encompassed hydrogen and kerosene storage tank modeling, addressing geometric, mechanical, and thermal properties, along with processes related to fueling and fuel consumption. A significant focus was placed on the visualization of SOFC powertrain integration and the placement of the hydrogen tanks within the aircraft, entailing a comparative analysis of various block shapes and tubular configurations during the analysis and design stages. Furthermore, the project involved an in-depth aerodynamic design analysis, prioritizing theoretical evaluation without necessitating physical modeling.

The paper is structured as follows: Sec. II describes the methodologies employed in the study, including the design framework, simulation tools, and comparative analysis techniques. This section details the aircraft sizing framework, propulsion system design, and integration processes, as well as the aerodynamic and weight modeling approaches. Section III presents the results and discussion, offering an analysis of the performance metrics for different aircraft configurations, including fuel consumption, emissions, and overall efficiency. Section IV concludes the study by summarizing the key findings and suggesting potential directions for future research in the field of hydrogen-powered aviation, emphasizing the development of more sustainable aircraft designs.

II. Methodology

The integration of an SOFC/GT propulsion system into a BWB aircraft demands a rigorous and methodical approach. This entails developing a comprehensive mission profile that accurately reflects typical operational conditions. This study explores the aerodynamic, propulsion, and structural facets of the design using weight estimations from NASA's Flight Optimization System Weights Estimation Method (FLOPS) and SOFC propulsion system design to conceptualize and evaluate the performance of this innovative initiative [12]. Subsequently, initial airframe and propulsion system dimensions are determined, and Open Vehicle Sketch Pad (OpenVSP) is employed to create a mesh, which is then utilized to configure visual representations in SolidWorks [13].

To facilitate a meaningful comparison, the widely adopted conventional Boeing 777-300ER and 737-800 aircraft are used as benchmarks. These models serve as references for evaluating the benefits and challenges associated with the incorporation of the hydrogen SOFC/GT propulsion system. By subjecting all aircraft to a consistent mission profile, which will be elaborated in the Results section, the comparative performance metrics are evaluated. Additionally, two capacities of aircraft configurations accommodating 365 passengers and 162 passengers, respectively, are assessed. Each capacity will include a conventional aircraft, hydrogen-powered BWB designs, and hydrogen-powered T&W configurations.

Ensuring safety is paramount in this study, necessitating a thorough examination of the aircraft's CG. The stability and control analysis is crucial for evaluating the overall safety and controllability of the aircraft, particularly when integrating a novel propulsion system. It is essential to note that, for a rigorous and fair comparison, an identical SOFC/GT propulsion system, scaled according to the specific power requirements of each aircraft, is utilized.

A. Aircraft Sizing Framework

The framework for defining aircraft geometries and weight estimation is illustrated in Fig. 1. Weight estimation methods from FLOPS are used to model and analyze the initial weight assumptions and power requirements for each aircraft configuration. These outputs were subsequently used for postprocessing evaluations.

The design process for a vehicle requires initial mission profile parameters, including range, payload, and flight conditions. These parameters, coupled with wing geometry and payload specifications, form the basis of the design process. The number of engines and their placement on the wing or fuselage are also determined at this stage. Cabin dimensions for BWB aircraft were determined using methods from [7] based on the fuselage layout and efficiency, which, based on the number of abreast seats, seat pitch, and the number of passengers, determines the number of bays required to accommodate the payload. The method also determines the necessary fixed passenger equipment (such as galleys, lavatories, and closets), thus establishing the cabin width and length.

Given the initial sizing parameters, aerodynamic forces are determined, including lift and drag. These are calculated using parameters such as the mean aerodynamic chord, cruise velocity, and wing loading. For the BWB and conventional T&W configurations, the maximum L/D ratios, which are 27 and 18, respectively, were used to calculate the fuel consumption using the Breguet–Range Equation [14]. These

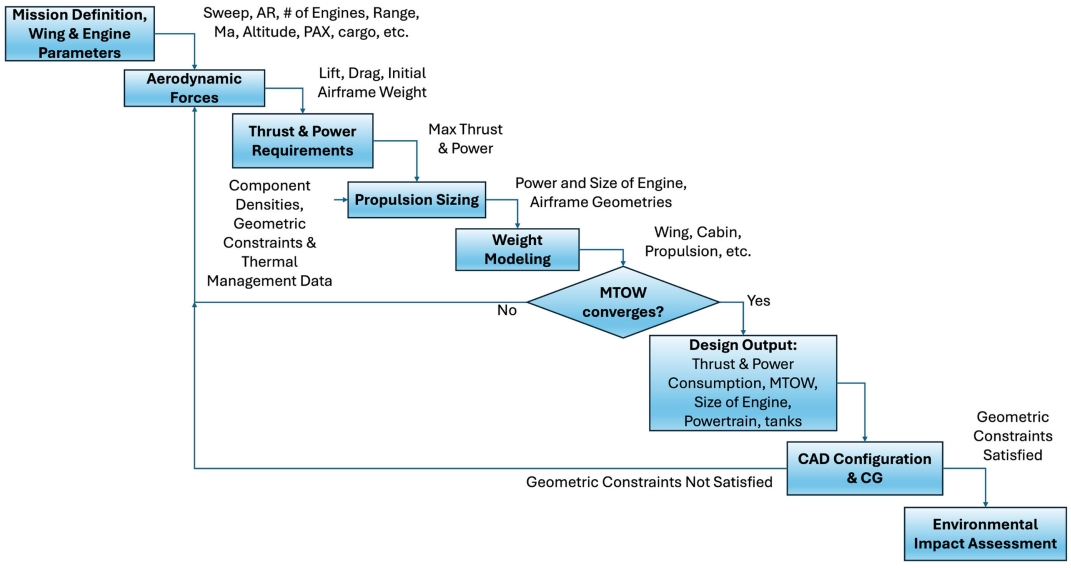

Fig. 1 Aircraft sizing framework.

coefficients are critical for determining the aircraft's aerodynamic efficiency and performance.

The results from the aerodynamic analysis, combined with liftoff acceleration derived from the takeoff field length and liftoff velocity from the mission profile, yield the maximum thrust per engine required for takeoff that is used in the propulsion system sizing. The rolling friction coefficient, obtained from relevant literature [15], is also considered in these analyses. Detailed methodologies for thrust and power estimations will be discussed in Sec. II.B.

Accurate weight estimation of the proposed aircraft is crucial, as the initial maximum takeoff gross weight (MTOW) significantly influences the power required from the engines. This, in turn, affects the minimum thrust required and the size of the hydrogen tanks and the corresponding SOFC/GT powertrain components, including the SOFC stacks, GT, cryo-cooler, battery, and high-temperature superconducting (HTS) motor.

The structural weight estimation process involves evaluating components such as the wing, fins, fuselage, landing gear, paint, and nacelles. Each component's weight is determined based on its dimensions, properties of materials, and structural requirements. The structural weight directly impacts the aircraft's performance and fuel efficiency. The systems and equipment weight group includes surface control systems, instruments, hydraulic systems, electrical systems, avionics, furnishings, and anti-icing systems. These control systems weight groups primarily takes into account factors such as MTOW, wing area, cabin floor area, and cruise range to provide an initial weight estimation. The propulsion system's weight estimation involves translating the required thrust into power output. This includes calculating the weight of the SOFC/GT powertrain components. These values, combined with the gravimetric and volumetric densities of the respective components, provide a preliminary weight estimation for the entire propulsion system. The operating items weight portion includes fixed equipment from the flight crew, miscellaneous passenger service weights, and cargo containers. These elements are essential for ensuring the aircraft's operational efficiency and serviceability. Finally, the iterative design process, by increasing the initial MTOW estimation at each step, will conclude upon achieving convergence at MTOW, marking the completion of the vehicle design process. Subsequently, it will proceed to the CG analysis and computer-aided design (CAD) configuration.

To ensure the accuracy of the model, validation tests were conducted, comparing the computed results against existing data from online sources. The discrepancies between the calculated MTOW and the reference values were found to be small, with deviations of 0.28% for the baseline BWB-450, 6.8% for the B777-300ER, and 0.46% for the B737-800. Below are the equations for each major weight group and the derivation for the MTOW. The breakdown of the various weight categories will be detailed in the Results section.

$$W_{\text{empty}} = W_{\text{structure}} + W_{\text{propulsion}} + W_{\text{systems}} \tag{1}$$

$$\text{OEW} = W_{\text{empty}} + W_{\text{op. items}} \tag{2}$$

$$\text{ZFW} = \text{OEW} + W_{\text{payload}} \tag{3}$$

$$\text{MTOW} = \text{ZFW} + W_{\text{fuel}} \tag{4}$$

B. Propulsion System Sizing

The methodology for determining thrust and power during various phases of flight involves a detailed set of equations that take into account specific flight conditions such as altitude and range. The method systematically dissects the various portions of the flight, namely, taxi, takeoff, climb, cruise, descent, and landing, following a predefined flight trajectory. Equations (5) and (6), coupled with the aircraft's remaining weight, parasitic drag, lift-induced drag, and compressible drag, were used to determine the thrust and climb/descent angle, denoted as γ, at each phase.

The power required for each aircraft configuration is fundamentally tied to the computation of the takeoff thrust. The maximum thrust, referred to as the takeoff thrust, is a function of the takeoff acceleration, as shown in Eq. (7). This equation also considers the aircraft takeoff gross weight, the number of engines, lift and drag forces, and rolling friction taken from the literature [15].

$$\text{Thrust} = D_{\text{total}} \quad \text{for cruise} \tag{5}$$

$$\text{Thrust} = (\text{Weight})\sin(\gamma) + D_{\text{total}} + \text{ma} \quad \text{for all others} \tag{6}$$

$$a_{\text{takeoff}} = \frac{V_{\text{takeoff}}^2}{2 \cdot \text{TOFL}} \tag{7}$$

where a_{takeoff}, V_{takeoff}, and TOFL represent takeoff acceleration, takeoff velocity, and takeoff field length in Eq. (7).

The power generated during takeoff is then computed as a function of the thrust force and takeoff velocity, as described in Eq. (8). This methodology ensures precise calculations of thrust and power tailored to different flight phases. The equations incorporate various dynamic factors such as lift, acceleration, rolling friction, and engine thrust to provide a complete analysis of the aircraft's performance throughout its operation.

$$\text{Power}_{\text{takeoff}} = \text{Thrust}_{\text{takeoff}} \times V_{\text{takeoff}} \tag{8}$$

1. *SOFC/GT System Design*

The SOFC/GT hybrid system depicted in Fig. 2 operates by using hydrogen from the cryogenic pressurized storage tank, which is pumped by the fuel pump and preheated in the fuel heater before entering the SOFC. Inside the SOFC, hydrogen electrochemically reacts with the oxygen in the air to produce electrical energy, water, and heat. The high-temperature exhaust gases from the SOFC are directed to the turbine, generating mechanical energy to drive the compressor and generator. The compressor increases the pressure of the incoming air, ensuring efficient operation at high altitudes. The exhaust heat is recovered by a recuperator, preheating the incoming air to improve overall system efficiency. A battery and electric motor help manage the power load and ensure stability in the system's electrical output. Following the power system schematic depicted in Fig. 2, its design must be refined to ensure compactness, efficient thermal distribution, and safety compliance. Historically, such systems have been configured in dense, engine-like structures, while others have adopted designs that allocate more space to individual components, resulting in larger overall volumes. Our design, conceptualized in Fig. 3, aims to optimize volume, mass, thermal efficiency, and electrical efficiency. This integration process includes a comprehensive analysis of the aircraft's CG, ensuring that it remains within safe operational limits and predefined envelopes.

The powertrain model design is adapted and modeled from previous work [16], which demonstrated its capability in responding to power profiles with the aid of a battery in MW-scale systems. The SOFC/GT technology has been extensively verified in both literature and commercial stationary power applications, and while not currently commercially available with fast dynamic response capabilities, it has been extensively evaluated for its ability to respond to dynamic changes while offering durability and a long operational lifetime [16–18]. This paper focuses on the design and integration of the SOFC/GT system within aircraft. The SOFC/GT system presents several challenges that need to be addressed. These include the placement of hydrogen tanks, insulation, leakage prevention, and thermal management of high temperatures. Specific design choices in this aircraft aim to mitigate these issues, ensuring the efficient and safe operation of the powertrain system. Only by addressing these and all other technical considerations, including some not addressed herein, like susceptibility to impact loading, can the SOFC/GT system be effectively integrated into aviation applications, paving the way for more sustainable power solutions in the industry.

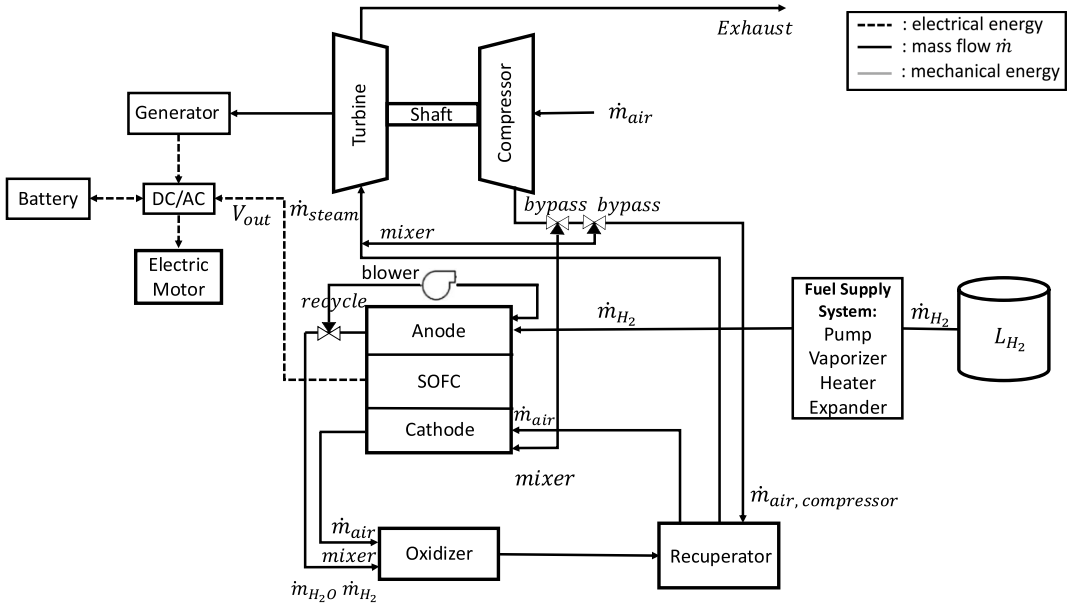

Fig. 2 Schematic of an SOFC/GT hybrid power system, illustrating the flow of electrical energy, mass, and mechanical energy.

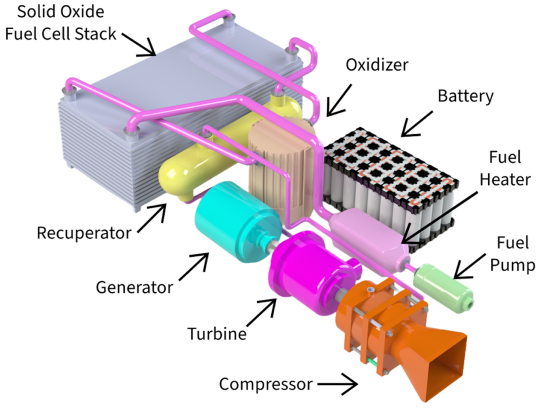

Fig. 3 CAD model of the SOFC/GT hybrid power system, showing the arrangement and integration of major components.

Table 1 Component densities of SOFC/GT powertrain

Parameter	Value
SOFC volumetric density, kW/kg	2.5
SOFC gravimetric density, kW/L	7.5
Battery volumetric density, kWh/L	0.67
Battery gravimetric density, kWh/kg	0.35
GT volumetric density, kg/m^3	8000
GT gravimetric density, kW/kg	4.4
SOFC/GT cycle efficiency, %	71.4

2. *SOFC/GT Weight Analysis*

For the conventional kerosene-powered B777-300ER and B737-800, the turbofan engine weight estimations from FLOPS were utilized. The lack of commercial components for complex hybrid powertrain systems, particularly in aviation applications where component weight is critical, contrasts with stationary power applications where SOFC/GT systems have been primarily utilized. The assumptions for weight analysis of these advanced concepts present in the literature make it challenging to settle upon specific values. Hence, this paper focuses on developing a methodology to examine the synergy of the BWB concept with hydrogen and fuel cell technology, highlighting potential benefits and challenges rather than performing a detailed mass analysis, which would require modeling and designing each component—a significant objective for future work. Currently, there is also limited to no comprehensive mass analysis for SOFC/GT systems, especially for aviation applications at megawatt (MW) scales. Table 1 lists the main assumptions for gravimetric energy density. The fuel cell, the heaviest component of the powertrain, references experimental work by NASA Glenn Research Center, achieving a 2.5 kW/kg density, at least twice the commercially available power density but still lower than current turbofans with a range of 3.33–10 kW/kg [3,19]. "Rather than heavy metal interconnects, Glenn's innovative bi-electrode-supported cell (BSC) uses a thin layer of electrically conductive $LaCaCrO_3$ (LCC) for current collection. To improve strength during thermal cycling and to simplify stack manufacture, its design is structurally symmetrical with a thin yttria-stabilized zirconia (YSZ) electrolyte supported on either side by a porous support structure" [20,21]. Moreover, Collins and McLarty estimate the net system power density of SOFC/GT for aviation to be 0.92 kW/kg [19]. Until recently, SOFC development has not focused on weight reduction, resulting in PEMFC and HT-PEMFC achieving better experimental claims and commercial applications, such as the fuel cell system of the Toyota Mirai, which claims a 4 kW/kg commercially.

Furthermore, the SOFC/GT system is sized to provide 75% of the takeoff power requirement (maximum power), while the battery provides 25%. In addition to the assumptions in Table 1 [16,19,22,23], individual components of the SOFC/GT powertrain presented later in the Results section are scaled based on the scaling factors from [3,19,23]. The net system power density of the SOFC/GT is estimated to be 1.5 kW/kg.

3. *HTS Motor and Nacelle Design for Hydrogen Powertrain*

The HTS motor design for the hydrogen powertrain uses assumptions from the N3-X motors [4,24]. Key parameters include a motor density of 29.14 kW/kg and a volumetric density of 100 kW/m^3, optimizing the balance between power output, weight, and volume [3]. The nacelle dimensions are scaled from N3-X specifications, with the average diameter assumed as

$$D_{\mathrm{NAC}} = \frac{50.6 \times (\mathrm{Power})}{5.74} \tag{9}$$

where D_{NAC} is the average scaled diameter of the nacelle and Power is the power output of the motor converted to the unit of MW.

The nacelle weight is

$$W_{\mathrm{NAC}} = 0.25 \times T_{\mathrm{NAC}} \times D_{\mathrm{NAC}} \times X_{\mathrm{NAC}} \times F_{\mathrm{Thrust}}^{0.36} \tag{10}$$

where W_{NAC} is the weight of the nacelle, T_{NAC} is a constant related to nacelle weight (unitless), D_{NAC} is the average scaled diameter of the nacelle, X_{NAC} is the average scaled length of the nacelle, and F_{THRUST} is the thrust force.

4. *Air Duct Design for Optimal Performance in Cruise and Taxi Phases*

Selecting the correct air duct dimensions is crucial for balancing operational requirements during cruise and taxi phases. Choosing an air velocity of 30 m/s for duct design accounts for high-speed airflow during cruise and low-speed requirements during taxi operations. A small blower ensures adequate airflow during ground operations. For an assumed fuel cell power output of $P = 45$ MW and an efficiency of $\eta = 0.714$, the hydrogen fuel consumption rate is modeled. The required airflow rate, based on a stoichiometric air-to-fuel ratio of 34.3, is determined. Given standard air density and an air velocity of 30 m/s, the duct cross-sectional area is found. Two rectangular ducts are proposed for the largest BWB configuration designed in this paper, each with a height of 30 cm and a width of 81.7 cm. These ducts are positioned on the sides of the aircraft, similar to some conventional designs, to minimize drag. During ground operations, a small blower provides the necessary airflow, ensuring the SOFC system remains operational to avoid very long startup times and durability concerns. Appropriate insulation can keep a shutdown SOFC warm enough over an entire 24 h period for a very quick startup [25].

5. *Thermal Management and Insulation for Cryogenic Hydrogen Storage Tanks*

The use of liquid hydrogen as a cryogenic fuel source introduces additional considerations. Advanced temperature-controlled fuel tanks are required to handle the cryogenic conditions. The choice of materials for these tanks, as well as for the propulsion components and wing structure, plays a significant role in determining the overall weight and stability of the aircraft. Material selection impacts not only the structural integrity and durability but also the thermal insulation properties essential for maintaining the hydrogen in a liquid state. Furthermore, following the simplified methodology from [26] for liquid hydrogen tank modeling for aircraft purposes, Fig. 4 portrays design choices. The analysis evaluates the thermal performance of vacuum insulation panels (VIPs) and multilayer insulation (MLI) for a cylindrical hydrogen storage tank by calculating the heat transfer through conduction, radiation, and convection. The tank dimensions and environmental conditions are specified, and the thermal properties of the insulation materials are considered. The analysis computes the heat transfer rates and the boil-off rates of hydrogen over a range of insulation thicknesses. Additionally, it analyzes the heat gain over time for a selected insulation thickness.

The methodology involves several key steps. First, the surface area of the tank (A_{tank}) is computed to include the cylindrical and hemispherical parts. The thermal resistances (R) for VIP and MLI are determined using their respective thermal conductivities and insulation thicknesses (t) [Eq. (11)]. The heat transfer due to conduction ($Q_{\mathrm{conduction}}$) is then calculated using Eq. (12). Radiation heat transfer ($Q_{\mathrm{radiation}}$) is considered using the Stefan–Boltzmann law [Eq. (13)]. Forced convection heat transfer ($Q_{\mathrm{convection}}$) is evaluated using the Nusselt number (Nu) which is derived from the Reynolds (Re) and Prandtl (Pr) numbers [Eqs. (15–17)]. Finally, the total heat transfer (Q_{total}) and the corresponding hydrogen boil-off rates are computed [Eq. (19)]. Thermal properties of the materials are considered constant and do not vary with temperature. The ambient temperature is assumed to be constant at 288 K. Forced convection is calculated using standard empirical correlations that are suitable for external flow over a cylinder. Additionally, the analysis is performed under steady-state conditions.

$$R = \frac{t}{k \cdot A} \tag{11}$$

$$Q_{\mathrm{conduction}} = \frac{T_{\mathrm{surface}} - T_{\mathrm{air}}}{R} \tag{12}$$

$$Q_{\mathrm{radiation}} = \alpha \cdot \sigma \cdot A \cdot (T_{\mathrm{surface}}^4 - T_{\mathrm{air}}^4) \tag{13}$$

$$Q_{\mathrm{convection}} = h \cdot A \cdot (T_{\mathrm{surface}} - T_{\mathrm{air}}) \tag{14}$$

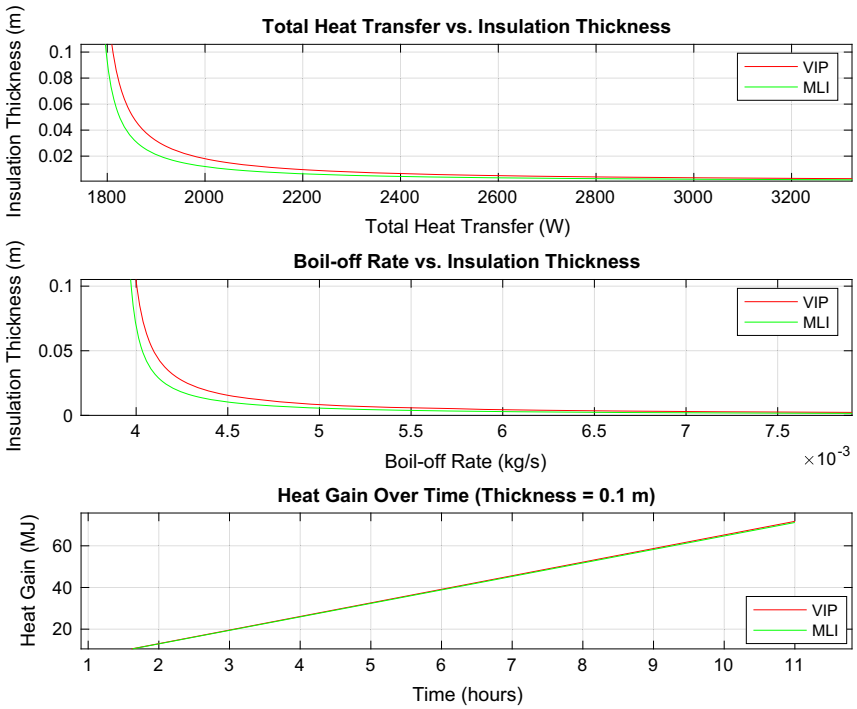

Fig. 4 Thermal performance of VIP and MLI insulation: total heat transfer, boil-off rate vs insulation thickness, and heat gain over time for 0.1 m thickness.

$$Re = \frac{\rho \cdot v \cdot L}{\mu} \tag{15}$$

$$Pr = \frac{c_p \cdot \mu}{k} \tag{16}$$

$$Nu = 0.644 \cdot Re^{0.5} \cdot Pr^{0.33} \tag{17}$$

$$h = \frac{Nu \cdot k}{L} \tag{18}$$

$$\text{Boil} - \text{off Rate} = \frac{Q_{\text{total}}}{\text{Latent Heat of Hydrogen}} \tag{19}$$

Figure 4 illustrates the methodology for designing tank insulation for an example cryogenic liquid hydrogen tank of 2916 kg, 9 m length, and 1.1 m diameter used in the hydrogen BWB-365. The top graph shows that increasing insulation thickness from 0.02 to 0.1 m reduces total heat transfer from approximately 2250 to 1750 W, with MLI performing better than VIP. The middle graph indicates that boil-off rates decrease from about 5 to 3.8 g/s with increased insulation thickness, with MLI showing lower rates than VIP. The bottom graph demonstrates that over 11 h, MLI results in cumulative heat loss of around 70 MJ, compared to slightly higher values for VIP. These results, supported by the thermodynamic model described above, underscore the importance of effective insulation in minimizing heat ingress and boil-off rates in cryogenic tanks and help with making informed tank design choices.

C. Simulation of Cryogenic Hydrogen Tank Operation

Hydrogen can be stored in liquid form by cooling it to cryogenic temperatures. Its liquefaction temperature is −252.78°C (20.37 K) at atmospheric pressure. Liquid hydrogen tanks need to be well-insulated to minimize vaporization losses, as external heat causes liquid hydrogen to turn into gas. Despite high-quality insulation, some vaporization will still occur due to heat inflow. When liquid hydrogen vaporizes, its specific volume increases significantly, expanding about 53 times from 0.0141 to 0.7507 m^3/kg at atmospheric pressure [27]. At all times, hydrogen will coexist as both liquid phase and gas phase within the tank. The vaporized gas from heat inflow raises the temperature and pressure inside the tank. Fuel consumption from the tank toward the fuel cell system acts as the pressure relief mechanism or otherwise boils off to the atmosphere [27]. The process of hydrogen boil-off, fuel consumption, and changes in temperature and pressure within a tank is modeled using the methodology described by [27,28].

The heat transfer coefficients for the liquid and gas regions of the storage tank are given along with the respective surface areas. The latent heat of vaporization and specific heat of GH_2 are also defined. For each time step, the heat transfer rates to the liquid and gas regions are calculated. The boil-off mass flow rate is computed based on the heat transfer rate to the liquid region. The mass changes for LH_2 and GH_2 are then updated using the mass flow rate of the fuel to the propulsion system and the boil-off rate. The internal energy change in the gas region is computed to update the temperature, and the pressure is updated using the ideal gas law.

The heat transfer rates $q_{\text{heat,liq}}$ and $q_{\text{heat,gas}}$ are calculated using

$$q_{\text{heat,liq}} = h_{\text{wall,liq}} A_{\text{liq}} (T_{\text{amb}} - T_{\text{liq}}) \tag{20}$$

$$q_{\text{heat,gas}} = h_{\text{wall,gas}} A_{\text{gas}} (T_{\text{amb}} - T_{\text{gas}}) \tag{21}$$

The boil-off mass flow rate $\dot{m}_{\text{boil}}$ is computed as

$$\dot{m}_{\text{boil}} = \frac{q_{\text{heat,liq}}}{L} \tag{22}$$

The mass changes for LH_2 Δm_{liq} and GH_2 Δm_{gas} are updated for each time step i, using

$$\Delta m_{\text{liq}} = -\dot{m}_{\text{boil}} \Delta t - \dot{m}_{\text{fuel,LH}_2} \Delta t \tag{23}$$

$$\Delta m_{\text{gas}} = \dot{m}_{\text{boil}} \Delta t - \dot{m}_{\text{fuel,GH}_2} \Delta t \tag{24}$$

The internal energy change ΔU_{gas} in the gas region is given by

$$\Delta U_{\text{gas}} = (q_{\text{heat,gas}} \cdot \Delta t + q_{\text{boil}} \cdot \Delta t - q_{\text{fuel,gas}} \cdot \Delta t) - (P \cdot (\dot{m}_{\text{boil}} + \dot{m}_{\text{fuel,GH}_2}) \cdot \Delta t) \tag{25}$$

The temperature T_{gas} and pressure P in the tank are updated iteratively, with pressure calculated using the ideal gas law:

$$P = \frac{n_{\text{GH}_2} R T_{\text{gas}}}{V} \tag{26}$$

where n_{GH_2} is the moles of GH_2, R is the gas constant, and V is the tank volume. The simulation results, including the mass of LH_2 and GH_2, temperature, and pressure over time, are plotted to analyze the system behavior. An example case study result can be found in the Results section.

This analysis of dynamic tank operation behavior has significant implications for flight operations and safety. The steady and controlled fuel consumption rates prevent rapid depressurization and temperature drops, ensuring that the hydrogen fuel system operates within safe thermal limits. The gradual temperature decrease and predictable pressure decline facilitate more efficient thermal management and reduce the risk of thermal stress on the tank materials, thus enhancing the overall reliability and longevity of the hydrogen storage system. Understanding these thermal and pressure dynamics is crucial for designing effective insulation and cooling systems that can handle the thermal loads during prolonged flight segments.

D. Center of Gravity and Airframe Configuration

The previously mentioned propulsion system sizing and weight models will generate an initial airframe geometry, alongside determining the volume of the SOFC/GT powertrain and dimensions required for hydrogen fuel tanks. Subsequently, the design process advances to ensure feasible integration of all aircraft components within the airframe to meet the CG requirements. This phase utilizes SolidWorks for physical placement, visualization, and CG analysis of the entire system. Should a component fail to fit within the airframe, it is imperative to revisit the initial aircraft sizing model to implement necessary modifications.

It is imperative to shield the hydrogen fuel tanks adequately while ensuring sufficient volume to support the defined mission, especially considering the tapering of the wing from root chord to tip. Equally critical is the aircraft's ability to satisfy CG requirements for all four loading scenarios, as shown in Eq. (27): 1) fully loaded with payload and fuel tanks, 2) fully loaded with payload and empty tanks, 3) empty payload with full tanks, and 4) empty payload and tanks. Compliance with these scenarios is essential as the aircraft routinely encounters each scenario, with noncompliance risking significant performance instability.

$$\text{CG} = \frac{\sum (x_{\text{component}} \cdot \text{weight}_{\text{component}})}{\sum \text{weight}_{\text{scenario}}} \tag{27}$$

where $x_{\text{component}}$ denotes the location of each component with respect to the origin defined, $\text{weight}_{\text{component}}$ is the weight of a specific component, and $\text{weight}_{\text{scenario}}$ is the total weight of each scenario.

E. Environmental Impact Assessment

To assess the environmental impacts of aviation, this section focuses on evaluating the gaseous emissions produced by aircraft propulsion systems. Key metrics used in this analysis include emissions indices for carbon dioxide (CO_2), water vapor (H_2O), carbon monoxide (CO), hydrocarbons (HCs), and nitrogen oxides (NO_x), quantified in kilograms per passenger nautical mile (kg/PAX-nmi).

Global warming potential (GWP) 100 values are applied to calculate equivalent CO_2 emissions, which account for the climate impact of non-CO_2 gases. Emissions for each flight segment are analyzed, with emission indices (EIs) determined based on stoichiometric equations and International Civil Aviation Organization (ICAO) databank values. Additionally, the potential formation of contrails is examined, comparing predictions for hydrogen-powered aircraft versus conventional kerosene-powered aircraft using a predictive model based upon water partial pressures. This comprehensive assessment aims to provide a detailed understanding of the environmental footprint of conventional aircraft and alternative-fueled aircraft during various flight segments.

To calculate the EIs for CO_2 and H_2O for different flight segments of the B777-300ER with GE90-115 engines and the B737-800 with CFM56-7B18 engines, we utilized ICAO databank [29] values for HC, CO, and NO_x emissions. The stoichiometric equation used to balance these emissions is given by

$$C_{12.5}H_{24.4} + aO_2 + bN_2 \rightarrow xCO_2 + yCO + zH_2O + wHC \quad (28)$$

For each flight segment, the mass of carbon in kerosene was distributed among CO, HC, and CO_2. The total mass of carbon in kerosene was calculated using the molar masses, and the carbon in CO and HC was determined based on their respective EIs. The remaining carbon was attributed to CO_2, and its mass was calculated accordingly. Similarly, the mass of hydrogen in kerosene was distributed among HC and H_2O, with the remaining hydrogen attributed to H_2O.

The mass of CO_2 was determined using the formula

$$\text{mass}_{CO_2} = \text{mass}_{C,CO_2} \times \left(\frac{M_{CO_2}}{M_C}\right) \quad (29)$$

where mass_{C,CO_2} is the remaining carbon mass attributed to CO_2, and M_{CO_2} and M_C are the molar masses of CO_2 and carbon, respectively. The EI for CO_2 was then obtained by dividing the mass of CO_2 by the mass of kerosene.

The mass of H_2O was determined using the formula:

$$\text{mass}_{H_2O} = \text{mass}_{H,H_2O} \times \left(\frac{M_{H_2O}}{2 \times M_H}\right) \quad (30)$$

where mass_{H,H_2O} is the remaining hydrogen mass attributed to H_2O, and M_{H_2O} and M_H are the molar masses of H_2O and hydrogen, respectively.

For fuel cell aircraft, it is established that the only byproduct is water vapor when fueled by pure hydrogen. However, the SOFC/GT system includes a combustor/oxidizer that raises the fuel cell exit flow temperature to about 1200K. It is fair to assume that some thermal NOx will form at this temperature, as established in the literature [30]. Hasanzadeh et al. demonstrated a similar SOFC/GT system operating with comparable combustion temperatures, showing an NOx emission rate of 1.2 kg NOx/MWh [30]. The study shows peak system temperatures of 1233°C (1496 K) at the combustor exit.

In comparison, a methane-powered SOFC/GT system has been documented to emit 0.04 kg/MWh (5 ppmv) of NOx, with an exhaust flow rate and temperature of 34 kg/s and 360°C, respectively [31]. Furthermore, results from Sinha et al. indicate 0.3 g NO_x/kg of methane for combustion at 1200 K, while He et al. report 5 g NO_x/kg fuel for combustion at 1200 K [32,33]. Moreover, Fuel Cell Energy's SOFC 250 kW system mentions values of 0.005 kg NOx/MWh for the SOFC stack [34]. Based on the reviewed data and to maintain consistency, our emissions model assumes 0.04 kg NOx/MWh as the most reasonable estimate based on after burner temperatures and exit flow temperatures. This translates to 0.94 g NOx/kg of hydrogen based on hydrogen's energy content and SOFC/GT system efficiency of 71.4%. This is significantly smaller than what is observed from data from the conventional aircraft at 14 g/kg kerosene.

Figure 5 illustrates a phase diagram of water vapor pressure versus temperature, comparing the saturation pressures of liquid water and ice with the mixing lines for conventional aircraft and hydrogen fuel cell aircraft. The saturation vapor pressures were calculated using the Goff–Gratch equations [35] [Eqs. (31) and (32)]. The Schmidt–Appleman criterion was then applied to derive the mixing lines for both types of aircraft, taking into account parameters such as ambient pressure, EIs, specific heat capacity, lower heating values, and efficiencies.

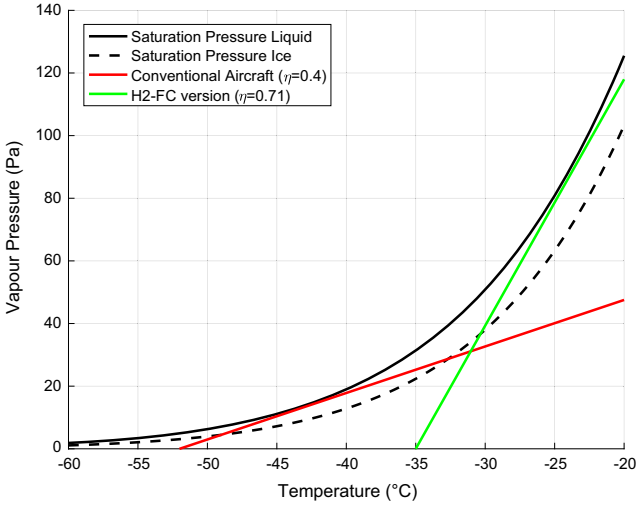

Fig. 5 Example Schmidt–Appleman criterion for assessing contrail formation for hydrogen FC and Jet-A at 40,000 ft.

$$P_{\text{saturation,water}} = \exp\Bigg(54.842763 - \frac{6763.22}{T} - 4.210\log(T) + 0.000367T + \tanh(0.0415(T - 218.8)) \times \Bigg(53.878 - \frac{1331.22}{T} - 9.44523\log(T) + 0.014025T\Bigg)\Bigg) \quad (31)$$

$$P_{\text{saturation,ice}} = \exp\Bigg(9.550426 - \frac{5723.265}{T} + 3.53068\log(T) - 0.00728332T\Bigg) \quad (32)$$

$$G = \frac{P \cdot EI_{H_2O} \cdot C_p}{\epsilon_{H_2O} \cdot \text{LHV} \cdot (1 - \eta)} \quad (33)$$

The Schmidt–Appleman criterion provides a framework for determining the atmospheric conditions conducive to contrail formation. According to this criterion, contrails form when the exhaust plume of an aircraft, which is initially hot and moist, mixes with the colder and drier ambient air. The mixing process must result in a supersaturated state with respect to water vapor, allowing for the condensation and subsequent freezing of water droplets, leading to contrail formation. When comparing contrail formation from hydrogen fuel cells and Jet-A fuel, several complex and interrelated factors come into play, like temperature, pressure, and humidity. Theoretical models, as illustrated in Fig. 5 below, demonstrate that the mixing slopes for hydrogen and Jet-A fuels differ significantly, indicating that contrails would form under distinct sets of atmospheric conditions. Hydrogen fuel cells, characterized by hydrogen's lower molecular weight, higher diffusivity, and higher efficiency, produce a steeper G-mixing line in the exhaust plume compared to hydrocarbon fuels. The values of G for conventional Jet-A fuel ($G_{\text{Jet-A}} = 1.4853$) and hydrogen ($G_{H_2} = 7.8655$) highlight this difference. Hence, hydrogen-fueled aircraft tend to form contrails at higher ambient

Table 2 Emission indices for different flight segments for conventional B777-300ER

Segment	HC EI, g/kg	CO EI, g/kg	NO_x EI, g/kg	CO_2 EI, g/kg	H_2O EI, g/kg
T/O (takeoff)	0.032	0.125	51.068	3147.5	1257.7
C/O (climb)	0.024	0.137	36.44	3147.5	1257.8
Approach	0.048	2.16	16.166	3144.3	1257.6
Idle	3.636	34.578	5.511	3088.9	1236.5
Cruise	0.012	0.07	40	3147.6	1257.8
Descent	0.018	0.5	20	3146.9	1257.8

Table 3 Emission indices for different flight segments for conventional B737-800

Flight segment	HC EI, g/kg	CO EI, g/kg	NO_x EI, g/kg	CO_2EI, g/kg	H_2O EI, g/kg
T/O (takeoff)	0.1	0.6	20.5	3146.7	1257.3
C/O (climb)	0.1	0.5	17.4	3146.8	1257.3
Approach	0.1	3.2	9.5	3142.6	1257.3
Idle	3.1	25.9	4.3	3103.2	1239.6
Cruise	0.05	0.3	15	3147.2	1257.6
Descent	0.2	1.5	7	3145.1	1256.7

temperatures compared to conventional Jet-A-fueled aircraft. This is primarily due to the higher water vapor EI of hydrogen combustion and the increased propulsion efficiency associated with hydrogen fuel cells [36].

The climate impact of contrails depends upon their persistence, which leads to the formation of contrail cirrus clouds. This persistence occurs when the ambient air's partial pressure of water vapor reaches or exceeds the ice saturation curve. The mixing trajectories depicted in Fig. 5 show that hydrogen and Jet-A fuels achieve ice saturation at different temperatures after initially reaching water saturation. This differential behavior underscores the unique conditions required for contrail formation with each type of fuel. Hydrogen's propensity to form contrails at higher temperatures is particularly notable, given its higher water vapor emission and efficiency metrics. In summary, while both hydrogen and Jet-A fuels can produce contrails, the specific conditions under which they do so vary due to differences in their emission characteristics and mixing dynamics with ambient air. Understanding these distinctions is crucial for assessing the potential climate impacts of transitioning to hydrogen fuel in aviation.

A summary of emissions indices determined for the different flight segments is presented in Tables 2 and 3. These tables provide detailed emissions indices of each flight segment for conventional aircraft. The data includes key metrics and is essential for understanding the environmental impact across different stages of flight. Note that environmental effects of water emissions cannot be fully explained by emissions indices alone. Contrail prediction models are needed for a more accurate assessment of their impact.

III. Results and Discussion

A. Mission Definition

In this paper, two distinct sample flight trajectories obtained from FlightAware [37] are utilized: one representing a journey from San Francisco International Airport (SFO) to Hong Kong International Airport (HKG) aboard a Boeing 777-300ER and the other from SFO to Boston Logan International Airport (BOS), as depicted in Figs. 6 and 7, respectively [37]. The objective is to assess the efficacy of the design and to evaluate and compare the correlation between the SOFC/GT powertrain and payload capacity across all studied aircraft configurations.

The flight profile from SFO to HKG was applied to the hydrogen-powered BWB-365 design as well as to both the hydrogen-powered T&W-365 and the kerosene-powered B777-300ER reference aircraft. For clarity, hydrogen T&W-365 refers to a retrofitted B777-300ER, essentially integrating the SOFC/GT powertrain and hydrogen storage

Fig. 6 Flight trajectory of example aircraft B737-800 from San Francisco International Airport (SFO) to Boston International Airport (BOS).

Fig. 7 Flight trajectory of example aircraft B777-300ER from San Francisco International Airport (SFO) to Hong Kong International Airport (HKG).

systems to produce power within the existing aircraft geometry. This naming convention is similarly applied to the hydrogen T&W-162. The flight trajectory from SFO to BOS was applied to our hydrogen-powered BWB-162, hydrogen-powered T&W-162, and the reference aircraft B737-800. These flight profiles serve as practical scenarios for evaluating the performance and efficiency of the proposed aircraft designs under real-world conditions.

The relative flight conditions and assumptions for these missions are detailed in Table 4. This includes considerations such as altitude, speed, payload, and fuel type, ensuring a comprehensive and rigorous comparison of the different aircraft configurations. By using actual flight data, we aim to provide a realistic assessment of the potential benefits and challenges associated with the integration of the SOFC/GT propulsion system in commercial aviation.

B. Aircraft Layout Comparison

The cabin and wing geometry were sized based on the passenger capacity required for specific flight profiles. This study divides the aircraft into two classes: one configuration accommodates 365 passengers, and the other accommodates 162 passengers. These numbers were derived from existing sources representing typical passenger capacities for reference aircraft [38]. Figure 8 provides a visual representation of the designed hydrogen-powered BWB-365.

The span of the designed aircraft is 62.2 m, with a root chord of 37.5 m. The overall shape and wing geometries, including aspect ratio (AR) and sweep angle, of the aircraft are based on the baseline BWB-450 [7], with the wing geometries scaled according to the payload requirements. Multiple wing designs were evaluated, and it was found that the design featuring a flat upper wing and centerbody was the most advantageous for arranging the cabin layout (three-class configuration) and hydrogen tanks. This specific design also offers significant potential for scalability, allowing the geometry to be adjusted according to different needs.

The hydrogen tanks, which come in three different dimensions, are cylindrical in shape for better pressure distribution and are located on each side of the wings. The sizing process and considerations for the hydrogen tanks take into account geometric constraints, thermal management, and material properties. Each accident or leak scenario is evaluated based on flammability limits, density,

Table 4 Mission definition assumptions per aircraft

Parameter	Hydrogen BWB-365	Kerosene B777-300ER	Hydrogen T&W-365	Hydrogen BWB-162	Kerosene B737-800	Hydrogen T&W-162
PAX	365	365	365	162	162	162
Cargo, kg	15,422	15,422	15,422	2268	2268	2268
Cruise, Ma	0.84	0.84	0.84	0.78	0.78	0.78
Cruise range, nmi	6574	6574	6574	2415	2415	2415

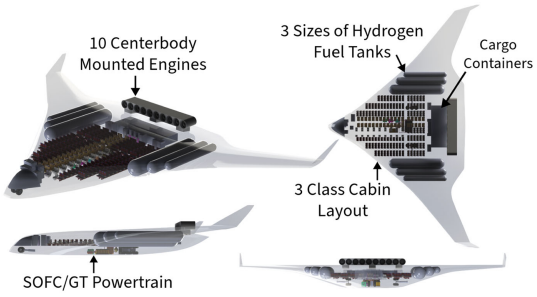

Fig. 8 Hydrogen BWB-365.

diffusivity, ignition energy, and the mixing of fuel and oxidant, among other parameters, to assess relative risk.

To balance the CG of the aircraft, the SOFC/GT powertrain was positioned 22.9 m from the tip of the aircraft, approximately half of the root chord length. Cargo containers are located in the back of the cabin, approximately 32.5 m from the tip of the aircraft, and the engines are mounted on top of the center aft body at 35.6 m from the tip of the aircraft. The hydrogen-powered BWB-365 features 10 engines, each scaled up from the N3-X model [4], providing a total power output of 59.9 MW.

The placement of all components was carefully chosen to satisfy the four critical aircraft CG cases: fully loaded payload and fuel tanks, fully loaded payload with empty tanks, empty payload with full tanks, and empty payload with empty tanks. An example of the CG calculation results is shown in Table 5.

To evaluate the stability of the aircraft, the CG of the wing was analyzed at positions ranging from 15 to 35% of the mean aerodynamic chord to determine if the overall CG location was acceptable.

Typically, adding a hydrogen fuel tank to a conventional tube-and-wing (T&W) aircraft requires sacrificing some cabin space to accommodate the additional length needed. Another option is to extend the fuselage to the required length to fit the fuel tank. In this case study, the goal was to preserve the payload capacity of the designed hydrogen-powered T&W aircraft. Therefore, in this paper, a fuselage extension of approximately 6.67 m to place the hydrogen fuel tank behind the cabin was selected. It is important to note that the wing geometry (AR and sweep angle) was preserved to be identical to the conventional B777-300ER.

Figure 9 illustrates the layout of the hydrogen fuel tank and the SOFC/GT powertrain in the modified B777-300ER. The powertrain components were strategically placed in front of the wing, at 25.4 m from the tip of the aircraft, to ensure the CG remains within an operable range.

Ten scaled engines, adapted from existing models, were mounted on the wings, providing a total power output of 53.1 MW. The cargo containers and fuel tank were positioned aft of the wing, at 54.7 and 72.2 m from the tip of the aircraft, respectively. This configuration

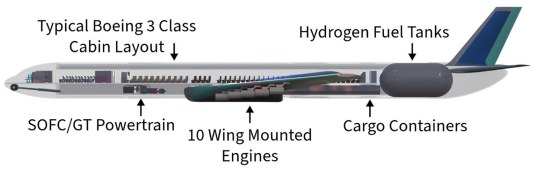

Fig. 9 Hydrogen T&W-365 side profile.

Table 5 Center of gravity for four different scenarios of hydrogen BWB-365

Parameter	Case 1: Full Cargo + PAX, Full Tank			Case 2: Full Cargo + PAX, Empty Tank		
Components	Weight, kg	Location, m	Moment, kg·m	Weight, kg	Location, m	Moment, kg·m
Nacelle + Pylon	3973.8	22.9	141308.3	3973.8	35.6	141308.3
Fuselage	57079.6	22.9	1304839.7	57079.6	22.9	1304839.7
Wing	27310.9	24.4	666517.8	27310.9	24.4	666517.8
Powertrain	38081.2	22.9	870536.2	38081.2	22.9	870536.2
Main Landing Gear	3558.5	25.4	90385.9	3558.5	25.4	90385.9
Nose Landing Gear	392.6	7.8	3050.2	392.6	7.8	3050.2
Fuel + Tank	22018.9	28.8	634193.8	0.0	28.8	0.0
Fixed Equipment	45490.5	24.4	1110187.8	45490.5	24.4	1110187.8
Passenger	44701.5	22.9	1021876.1	44701.5	22.9	1021876.1
Cargo	18279.8	32.5	594311.5	18279.8	32.5	594311.5
Sum:	260887.2			238868.3		
CG [% of MAC]:	25.3			24.9		
	Case 3: Empty Cargo + PAX, Full Tank			Case 4: Empty Cargo + PAX, Empty Tank		
Components	Weight, kg	Location, m	Moment, kg·m	Weight, kg	Location, m	Moment, kg·m
Nacelle + Pylon	3973.8	35.6	141308.3	3973.8	35.6	141308.3
Fuselage	57079.6	22.9	1304839.7	57079.6	22.9	1304839.7
Wing	27310.9	24.4	666517.8	27310.9	24.4	666517.8
Powertrain	38081.2	22.9	870536.2	38081.2	22.9	870536.2
Main Landing Gear	3558.5	25.4	90385.9	3558.5	25.4	90385.9
Nose Landing Gear	392.6	7.8	3050.2	392.6	7.8	3050.2
Fuel + Tank	22018.9	28.8	634193.8	0.0	28.8	0.0
Fixed Equipment	45490.5	24.4	1110187.8	45490.5	24.4	1110187.8
Passenger	0.0	22.9	0.0	0.0	22.9	0.0
Cargo	0.0	32.5	0.0	0.0	32.5	0.0
Sum:	197906.0			175887.1		
CG [% of MAC]:	25.0			24.4		

ensures that the cabin layout remains identical to that of the conventional B777-300ER, preserving passenger and cargo space.

By extending the fuselage and carefully positioning the hydrogen fuel tank and powertrain components, we aimed to maintain the operational capabilities and efficiency of the aircraft while integrating the hydrogen propulsion system. This design approach allows us to explore the potential of hydrogen-powered aviation without compromising on payload capacity or passenger comfort.

This paper also aims to conduct a comparative analysis of the performance of the designed aircraft for shorter flight durations and a smaller number of passengers. Both the hydrogen BWB-162 and B737-800 were evaluated for a cruise range of 2415 nmi and a passenger capacity of 162. The aircraft's span, based on its passenger capacity, was determined to be 34.5 m, with a root chord of 16.5 m. The hydrogen fuel tanks depicted in Fig. 10 represent the required fuel volume for completing the flight mission while maintaining a fixed cargo weight. Notably, Fig. 10 does not visually represent the maximum dimensions of the fuel tanks. This specific wing geometry allows for larger tanks to be accommodated, offering flexibility to increase the cruise range or enhance the payload capacity. Furthermore, the figure illustrates that the current positioning of cargo containers is between the cabin and hydrogen fuel tanks. Should larger tanks be required for extended or heavier missions, the cargo containers can be relocated to the bottom of the cabin, ensuring the CG remains within acceptable limits across all scenarios. Additionally, the proposed hydrogen BWB-162 incorporates a pivot gear design pioneered by JetZero for commercial BWB aircraft [39]. This design significantly reduces the airframe's overall size by placing cargo containers on each side of the cabin. JetZero also claimed that the innovative landing gear design features a fully passive motion system that enhances braking effectiveness by 30%. Similar to the approach taken with the hydrogen BWB-365, the placement of the SOFC/GT powertrain was strategically chosen to satisfy the CG requirements for all four scenarios effectively.

Lastly, the hydrogen T&W-162, shown in Figure 11, has the same geometry attributes based on the B737-800 and follows a similar design pattern to that of the hydrogen-powered B777-300ER. To preserve the chosen payload capacity, the fuselage was extended by approximately 2 m to accommodate the additional length required by the hydrogen tanks. This extension ensures that the hydrogen fuel tanks can be integrated without sacrificing passenger or cargo space.

The aircraft features four wing-mounted engines, collectively producing a total power output of 10.2 MW. The cabin layout, including the same number of passenger service equipment such as galleys, lavatories, and closets, remains identical to that of a conventional B737-800. This design decision was made to maintain the same level of passenger comfort and operational efficiency as the conventional aircraft.

By extending the fuselage and carefully integrating the hydrogen fuel tanks and powertrain components, we aimed to balance the innovative hydrogen propulsion system within the existing structural and operational requirements of the B737-800. This approach allows us to explore the viability of hydrogen-powered aviation while preserving the essential characteristics and performance of the aircraft.

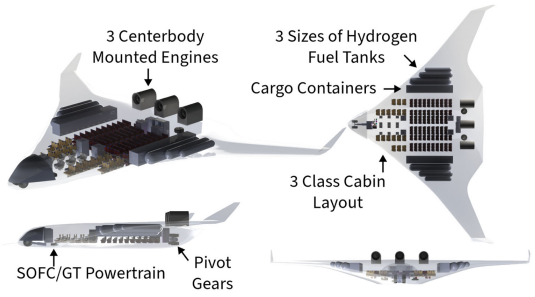

Fig. 10 Hydrogen BWB-162.

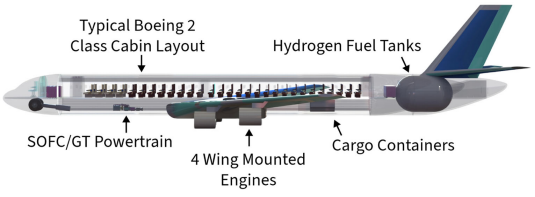

Fig. 11 Hydrogen T&W-162 side profile.

C. Simulation of Cryogenic Hydrogen Tank Operation for an Example Mission

In the simulation results presented in Fig. 12, the hydrogen boil-off, fuel consumption, temperature, and pressure change process in a tank over the flight duration of 11 h is modeled. Initial conditions include the liquid hydrogen (LH_2) mass and gaseous hydrogen (GH_2) mass calculated based on a 2916 kg total hydrogen load and a 7.2% GH_2 fraction.

The dynamic tank operation plots in Fig. 12 illustrate the mass of hydrogen, gaseous temperature, and tank pressure over time during an example flight of the hydrogen BWB. Due to the lengthy cruise phase (9.5 h) compared to other flight segments, the fuel consumption rate appears constant. The average fuel flow rates to the propulsion system for each section are as follows: for the taxi phase, the flow rate is 0.00693 kg/s; for the takeoff phase, it is 0.092589 kg/s; for the climb phase, the rate is 0.08316 kg/s; during the cruise phase, the flow rate is 0.0693 kg/s; and for the descent phase, the flow rate is 0.04851 kg/s. The plot shows the mass of hydrogen, with the total mass displaying a consistent decline, reflecting nearly steady consumption on average.

The system experiences a heat flux of approximately 10 W/m^2. As hydrogen is discharged, the available volume in the tank increases, causing the gaseous hydrogen pressure to expand into this larger volume. This expansion leads to a pressure drop within the tank, which is accompanied by a corresponding decrease in temperature, as described by the ideal gas law. The steady decline in tank pressure from about 0.65 to 0.55 MPa, along with the gradual decrease in gaseous temperature from approximately 30 to 24 K, reflects the cooling dynamics associated with hydrogen consumption and phase change [40]. Notably, the mass of gaseous hydrogen remains relatively constant throughout the flight because it is primarily the liquid hydrogen that is vaporized and consumed. This counterintuitive result, considering the fact that heat gain and boil-off are usually a concern for liquid hydrogen storage, can be observed from Fig. 12, which illustrates the steady-state behavior of gaseous hydrogen mass despite ongoing consumption and phase transition processes with concurrent heat gain from the environment. Understanding the natural boil-off and consumption behavior, along with tank insulation modeling as illustrated in Fig. 4, aids in making design choices that balance natural boil-off with the boil-off that will be effectively utilized by the aircraft. The 36 m^3 tank is designed with a 4 g/s natural boil-off based on results from Fig. 4 with a 10 cm MLI insulation. For reference, the lowest fuel flow rate during taxi for the BWB-365 flight case study is 6.93 g/s, meaning that no fuel will be vented to the environment. Given that the SOFC will remain constantly operational, it is unnecessary to design tanks with additional insulation, which would add unnecessary weight and volume.

D. Hydrogen vs Conventional Aircraft Comparison

Figure 13 illustrates the comparison between the OEW, shown in blue bars, and the combined payload and fuel weight, depicted in orange bars, for all six aircraft configurations. It is important to note that the fuel type used in this comparison is consistent with the naming convention of each column in Fig. 13. The payload for each aircraft is identical within their respective classes, as detailed in Table 6.

For the 365-passenger class, the hydrogen BWB-365 design exhibits a lower MTOW compared to the conventional B777-300ER using Jet-A fuel. However, it remains 10% heavier than the retrofitted hydrogen T&W-365. Conversely, the MTOW of the

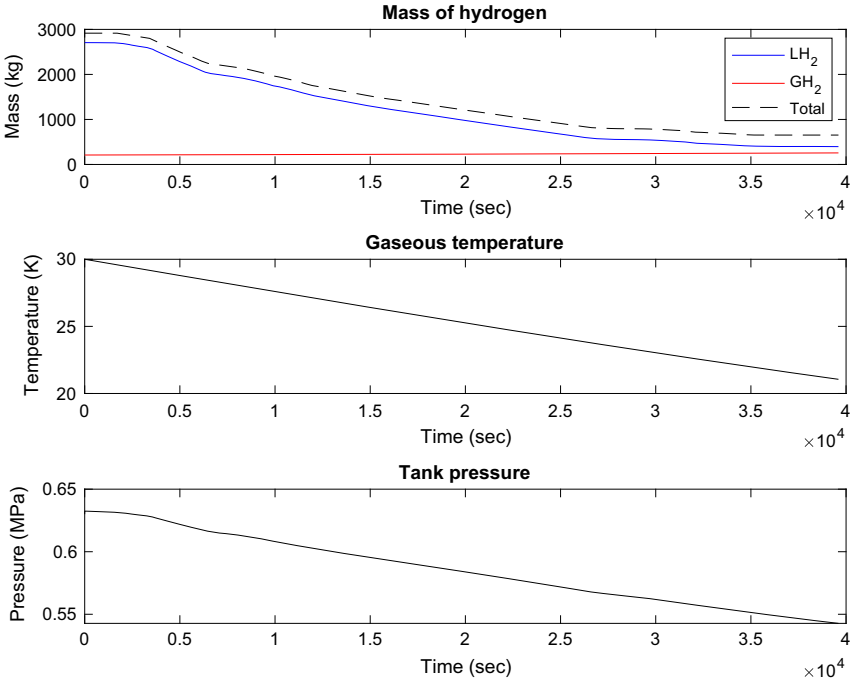

Fig. 12 Dynamic tank operation during cruise phase for 2916 kg H_2 tank with changing average consumption rate of 69.3 g/s for example flight trajectory from SFO to HKG.

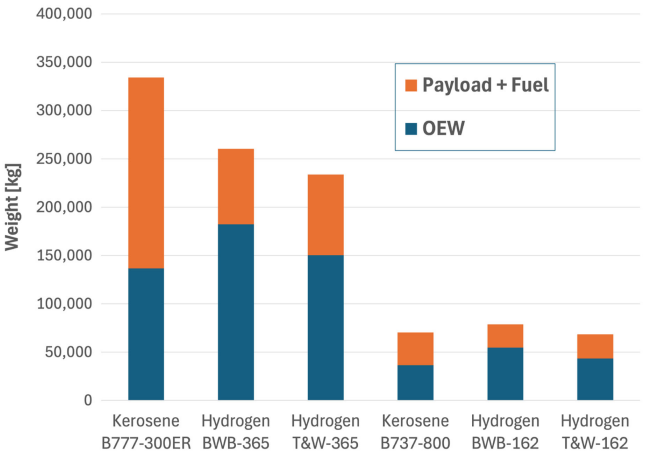

Fig. 13 Operating empty weight and combined payload and fuel weight bar chart for all six studied aircraft configurations.

hydrogen BWB-162 surpasses both the retrofit hydrogen T&W-162 and the conventional B737-800.

A notable trend across both classes is the progressive increase in OEW, ascending from conventional baseline aircraft to hydrogen baseline aircraft and finally to the hydrogen BWB configurations. To scrutinize the causes of this OEW increase, Table 7 presents a detailed MTOW breakdown for the hydrogen T&W-365 and hydrogen BWB-365, and Table 8 describes the weight proportion of each components in the SOFC/GT powertrain.

Due to a higher aerodynamic coefficient and the enhanced performance efficiency, the fuel weight for the BWB is expected to be lower than that of a conventional T&W configuration. Within the aircraft empty weight category, the propulsion weight groups and structural weight groups for the hydrogen BWB-365 are more significant compared to those of the hydrogen T&W-365. The weight of all components within the SOFC/GT powertrain was calculated based on the power required for each aircraft. Specifically, the hydrogen BWB-365 requires 12.7% more power output compared to the hydrogen T&W-365. Consequently, it is natural to observe a higher propulsion weight, because the fuel cell system has much lower power density compared to a GT, so that a larger system is needed to generate the necessary power.

In the structural weight group, the wing of the hydrogen BWB-365 is approximately 12,000 kg heavier. This increase is primarily attributed to a larger wing area, increased control surfaces area, and an additional aft body weight portion, which is a function of the cabin planform area—36% higher in the BWB configuration. Despite the longer length of the T&W configuration, the centerbody weight of the hydrogen BWB-365 is higher due to the overall increase in cabin planform area. This increase in surface area for the BWB configuration aligns with findings in the literature [14]. Kimmel and Bradley also observed a similar trend in OEW growth for the BWB design [7].

Table 6 Comparison of performance metrics between hydrogen- and kerosene-powered aircraft configurations under different operational scenarios

Parameter	Kerosene B777-300ER	Hydrogen BWB-365	Hydrogen T&W-365	Kerosene B737-800	Hydrogen BWB-162	Hydrogen T&W-162
No. of engines	2	10	10	2	3	4
Total power, MW	77.96	59.9	53.1	10.74	11.91	10.2
TOGW, kg	334211	260887	234776	70307	78780	68387
OEW, kg	136559	183045	151307	36334	54648	43441
Payload weight, kg	60124	60124	60124	22108	22108	22108
Fuel weight, kg	137522	18003	23346	11859	2027	2842
Weight per PAX, kg	916	714	643	434	486	422
Payload + Fuel, kg	197646	78126	83470	33968	24135	24950

Table 7 Detail weight breakdown of hydrogen BWB-365

					Parameters	Hydrogen T&W-365	Hydrogen BWB-365
					Average cruise L/D	15	23.4
				Structural Weight	Wing [kg]	14305.4	26087.2
					Empennage [kg]	4180.2	--
					Centerbody [kg]	--	57079.6
					Fuselage [kg]	35561.2	--
					Landing Gear [kg]	3972.5	3951.1
					Fins [kg]	--	1223.7
					Nacelle [kg]	1260.1	1316.4
					Paint [kg]	3776.8	2081.7
					Total [kg]:	63056.2	91739.8
			Aircraft Empty Weight	Propulsion Weight	SOFC [kg]	15940.2	17981.5
					Battery [kg]	4953.6	5588.0
					Gas Turbine [kg]	2768.5	3123.0
					Cryo-cooler [kg]	1619.0	1828.1
					HTS Motor [kg]	1821.6	2056.9
					Thrust Reverser [kg]	1221.3	1379.1
					Hydrogen Tanks [kg]	5441.0	4073.0
					Other Components [kg]	7757.3	8781.9
					Total [kg]:	41522.5	44811.5
				Systems & Equip. Weight	Surface Control Sys. [kg]	1675.3	2890.9
					Instruments System [kg]	1517.0	2069.9
					Hydraulic System [kg]	1921.9	3168.3
					Electrical System [kg]	4665.8	4102.2
					Avionics System [kg]	4790.6	5815.2
					Furnishings [kg]	23136.3	19329.1
					Anti-icing System [kg]	201.7	237.0
					Total [kg]:	37908.7	37612.6
					WEMPTY [kg]:	142487.4	174163.9
				Operating Items Weight	Fixed Equipment [kg]	1959.5	1959.5
					Passengert Service [kg]	3836.6	3836.6
					Cargo Containers [kg]	2857.6	2857.6
					Total [kg]:	8653.8	8653.8
					WOPIT [kg]:	8653.8	8653.8
					OEW [kg]:	151141.2	182817.6
					Payload [kg]	60123.6	60123.6
					ZFW [kg]:	211264.8	242941.3
					Fuel [kg]:	23228.8	17945.9
Maximum Takeoff Gross Weight					MTOW [kg]:	234776.5	260887.2

Table 8 SOFC/GT components' breakdown mass and percent of total mass for 45 MW SOFC/GT and 3.75 MWh battery

Component	Mass, kg	% of mass
SOFC	17970	60.18
GT	3123	10.46
Compressor	226	0.76
Recuperator/HX	4199	14.06
Oxidizer/combustor	2524	8.45
Recycling blower	337	1.13
Air blower	112	0.38
Electric generator	474	1.59
Fuel pump	163	0.55
Fuel heater	163	0.55
Hydrogen delivery system (pump + tank flow conditioning + tubing)	569	1.90
Total power train mass	29860	100.00
Battery, kWh	5588	
Total with battery	35448	

The tank design for hydrogen storage in aviation achieves a finely balanced structural integrity, thermal efficiency, and weight optimization, aligning with stringent aerospace requirements. The tank wall thickness is carefully derived from specific geometry and selected materials, notably aluminum (4.4% Cu) 2014-T6, chosen for its high strength-to-weight ratio and fatigue resistance as well as low cost. Insulation is achieved through evacuated aluminum foil and fluffy glass mats as recommended by Rivard et al., which reduce thermal conductivity and hydrogen vaporization [41]. The factor of safety (FOS), set at 1.3, judiciously balances durability and material efficiency.

The resulting weight proportion of LH_2 for the designed tank systems varies across different aircraft configurations, specifically the hydrogen BWB-365, T&W-365, BWB-162, and T&W-162. These configurations have $W_{\text{tank}}/W_{\text{fuel}}$ ratios of approximately 0.227, 0.234, 0.244, and 0.221, respectively, corresponding to average tank efficiencies of 77.3, 76.6, 75.6, and 77.9%. The ratios provided above are the average efficiency of the six tanks combined for the respective BWB configuration. These tailored designs aim to balance storage capacity and structural weight according to the specific operational and performance needs of each model. This calculated ratio falls within the 15–30% range reported in the literature [42], which implies an optimized design using common materials. Gravimetric efficiencies in other research vary widely from 40 to 80% [43], with some designs approaching 73% efficiency [44]. This range indicates that the tank design in this study falls within a feasible scope, and differences in tank efficiency notably impact both power output and takeoff gross weight, as shown in Table A1 in the Appendix, which compares tank efficiencies ranging from 77 to 37% alongside the corresponding total power requirements and takeoff gross weights for the aircraft.

Table 8 provides a detailed mass breakdown of the components for a 45 MW SOFC/GT system coupled with a 15 MW, 3.75 MWh battery used in the BWB-365. Table 8 lists each component along with its mass. The SOFC is the heaviest component at 17,970 kg, followed by the recuperator/heat exchanger at 4,199 kg, and the GT at 3,123 kg. Other components like the oxidizer/combustor, recycling blower, and hydrogen delivery system also contribute to the total

mass. The total mass is 29,860 kg, and with the battery included, the total mass reaches 35,448 kg. Table 8 provides a more granular view of the SOFC/GT system components, while the overall propulsion system breakdown is depicted in Table 7.

Figure 14 illustrates the relationship between OEW and seating capacity for various aircraft models, including hydrogen-powered BWB designs. The hydrogen BWB-365 shows 34 and 21% higher OEW compared to the B777-300ER and the hydrogen T&W-365. This increase in OEW is partly due to the noncircular pressurized body of the BWB, which requires more structural material to maintain integrity, a larger area of the cabin, greater airfoil thickness to achieve higher lift, a unique landing gear configuration, and the weight of hydrogen storage systems and the SOFC/GT powertrain. Additionally, the BWB is overall a larger aircraft, which inherently requires more material and structural support, further increasing the OEW.

Previous alternative analyses of BWB have produced different conclusions, with some claiming lower and others higher TOGW than T&W aircraft. Adler and Martins determined that the hydrogen combustion BWB is 13% lighter MTOW than the hydrogen T&W counterpart and with lower fuel consumption, yet still the wing is 19% heavier [5]. Sgueglia et al. conducted a comparative analysis of the A320 Neo and three BWB baselines [45]. In all cases, the MTOW and the OWE of BWB were greater than those of the reference aircraft, primarily due to the centerbody structure. The more complex design necessitates reinforcements to handle pressurization and the bending moment of the outer wing, resulting in a heavier structure compared to a tubular fuselage, despite that fuel consumption is 18% lower in the best case [45]. Another comparison done by Reist and Zingg arrives at the conclusion that BWBs are more aerodynamically efficient than T&W's but are heavier, reducing the expected benefits in drag and fuel burn [46]. Regional and narrow-body BWBs show minimal fuel-burn reduction compared to T&W's [46]. Hence, the literature is inconclusive regarding whether a BWB aircraft is heavier than its T&W counterpart but consistently concludes, together with the current study, that BWB provides fuel savings due to the higher L/D and better aerodynamic efficiency.

Figure 15 compares fuel consumption per passenger-kilometer against seating capacity. Hydrogen aircraft models exhibit significantly lower fuel consumption per passenger-kilometer than conventional aircraft, such as the A320 and B777-300ER. This highlights the efficiency advantage of hydrogen power, leveraging its higher energy density to achieve lower fuel consumption metrics. Furthermore, hydrogen BWB has even further fuel/PAX-km savings compared to T&W aircraft despite the initial weight penalty and larger size of the BWB design with combined aerodynamic and propulsion efficiency benefits. This is consistent with other BWB designs, such

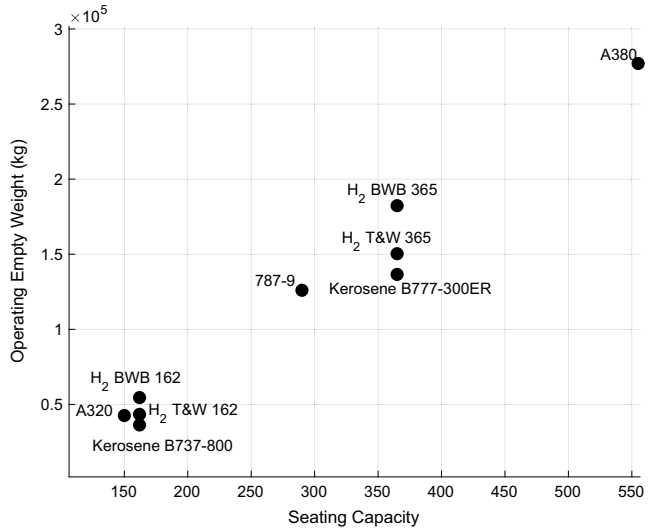

Fig. 14 Operating empty weight for BWB's and various hydrogen and conventional aircraft models.

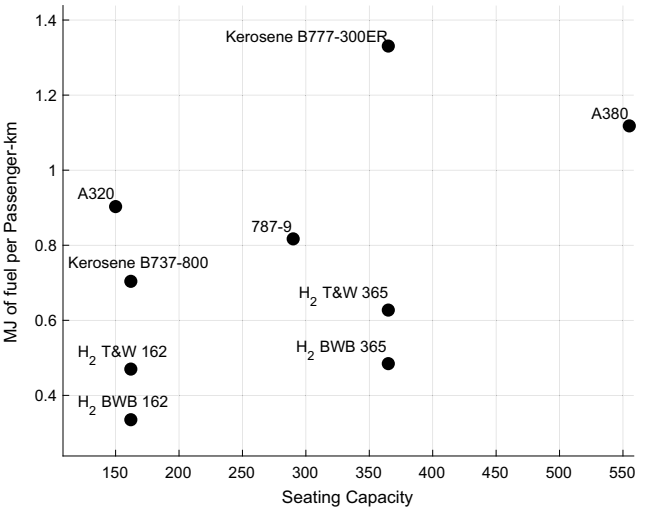

Fig. 15 Fuel consumption per passenger-kilometer of BWB's and various hydrogen and conventional aircraft models.

as Liebeck, demonstrating that a BWB designed for around 800 passengers and a range of 7000 nmi achieves a 27% reduction in fuel consumption per passenger-kilometer compared to a conventional aircraft using Jet-A fuel [14].

Key results reveal that scaling down from the hydrogen BWB-365 to the hydrogen BWB-162 resulted in unexpectedly positive outcomes. The weight per passenger for the hydrogen BWB-162 was 486 kg, compared to 714 kg for the hydrogen BWB-365, representing a reduction of approximately 31.9%. Additionally, the fuel consumption per passenger-kilometer decreased significantly, with the hydrogen BWB-162 achieving a 30% reduction compared to its larger counterpart. These improvements underscore the potential for hydrogen propulsion systems to enhance operational efficiency across different aircraft sizes.

One possible scientific explanation for these results is the square-cube law, which states that as a shape grows in size, its volume increases faster than its surface area. This leads to disproportionate increases in structural weight and aerodynamic drag for larger aircraft. In the case of the hydrogen BWB-162, the reduced size may result in more efficient aerodynamics, lower structural weight, and more favorable wing loading, thereby improving overall weight and fuel efficiency per passenger. Additionally, the hydrogen BWB-365's higher range necessitates larger and heavier tanks, which could contribute to the less favorable weight and efficiency metrics observed in the larger aircraft. The reduced structural requirements and optimized design approaches possible with the smaller hydrogen BWB-162 likely further enhance these efficiency gains.

E. Environmental Impact Assessment

Figure 16 presents a comparative analysis of the emissions composition by flight phase for conventional (777-300ER, 737-800) and hydrogen-powered (BWB-450 & T&W-365 and BWB-162 & T&W-162) aircraft models, highlighting significant differences in environmental impact. The pie charts show that for conventional models like the Boeing 777-300ER and Boeing 737-800, the cruise phase is the predominant contributor to emissions, particularly CO_2, H_2O, and NO_x. For instance, during the cruise phase, the Boeing 777-300ER emits 414,160 kg of CO_2 and 165,500 kg of H_2O, with 5,263 kg of NO_x. In contrast, during the taxi phase, the emissions are significantly lower, with the Boeing 777-300ER emitting 282 kg of CO_2, 112.9 kg of H_2O, and 0.503 kg of NO_x. Notably, CO emissions during taxiing are relatively high at 3.158 kg due to incomplete combustion at lower engine power settings typical of ground operations.

The hydrogen-powered models (BWB-365 & T&W-365 and BWB-162 & T&W-162) demonstrate significantly reduced emissions. However, hydrogen-fueled aircraft, with a higher watervapor EI and greater propulsion efficiency, produce a steeper G-mixing line ($G_{H2} = 7.8655$)

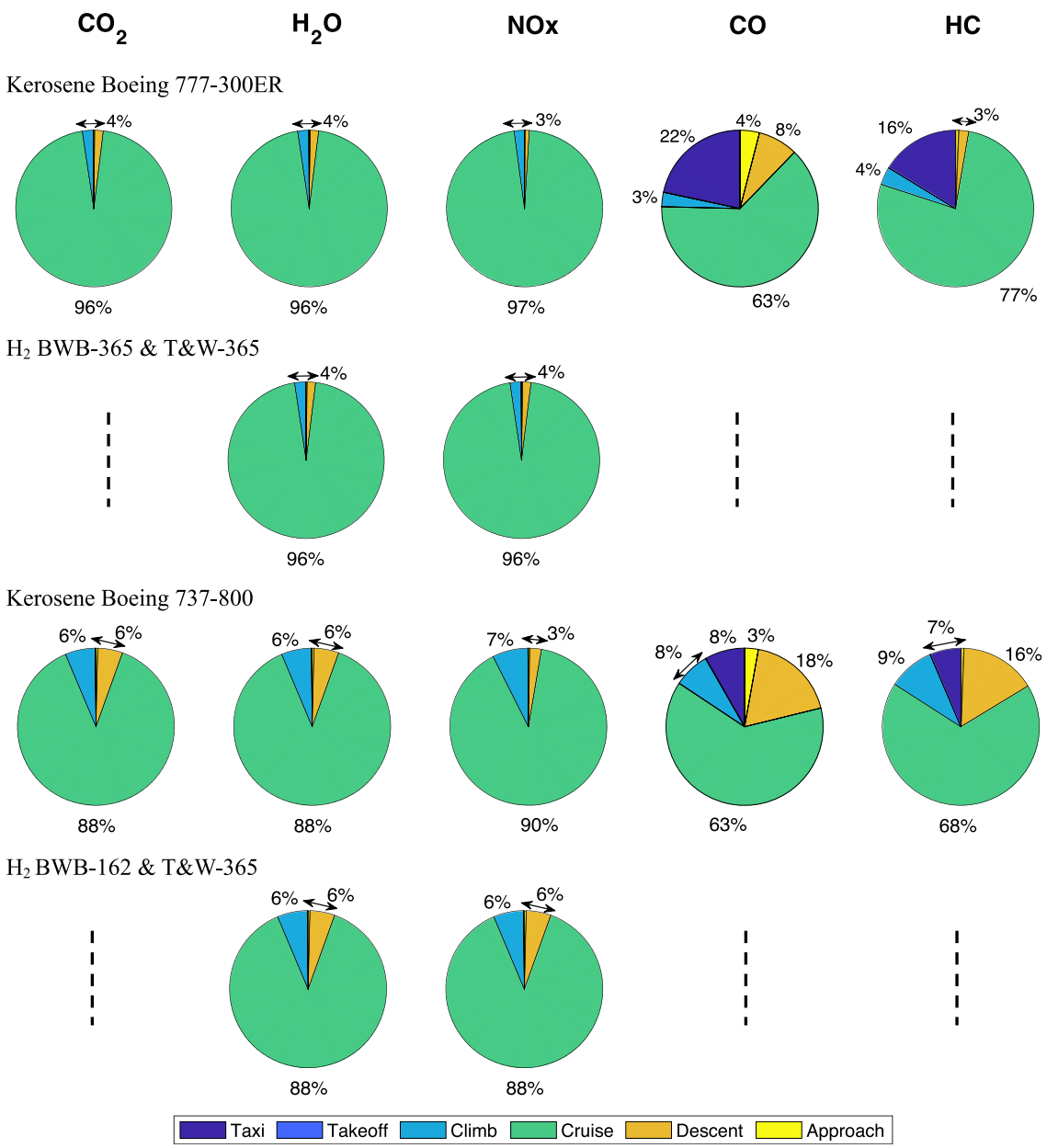

Fig. 16 Emission composition for the flight phase for conventional (777-300ER, 737-800) and hydrogen-powered (BWB-365 & T&W-365, BWB-162 & T&W-162) aircraft models.

compared to kerosene-fueled aircraft ($G_{Jet\text{-}A} = 1.4853$), as shown in Fig. 5. Consequently, hydrogen-powered aircraft tend to form contrails at higher ambient temperatures. For the BWB-450, H_2O emissions are highest during the cruise phase at 154,534.90 kg, while NO_x emissions during the same phase are significantly lower at 16.35 kg. In the taxi phase, H_2O emissions are 107.25 kg, and NO_x emissions are nearly negligible at 0.01 kg. Similarly, the BWB-162 shows substantial reductions in emissions, with H_2O emissions during the cruise phase at 16,150.5 kg and NO_x emissions at 1.71 kg, compared to the taxi phase, which has 24.38 kg of H_2O and no measurable NO_x emissions. More details for the breakdown of emissions are found in Tables B1–B4 in the Appendix. These results underscore the significant potential of hydrogen-powered aviation to reduce GHGs and other pollutants, thereby offering a more sustainable alternative to traditional jet fuel.

Figure 17 presents a comparison of total emissions (CO_2, H_2O, NO_x, CO, HC) for various aircraft models, including both conventional (777-300ER, 737-800) and hydrogen-powered configurations (BWB-365, BWB-162, T&W-365, T&W-162). This comparative analysis highlights that hydrogen-powered aircraft generally emit significantly lower CO_2 and NO_x compared to kerosene-powered models. Specifically, the hydrogen BWB-162 model exhibits the lowest total emissions, particularly noteworthy for its minimal NO_x emissions. To illustrate further, the total emissions for the kerosene-powered 777-300ER show a significant amount of CO_2 (432780 kg) and NO_x (5431.6 kg). In contrast, the hydrogen BWB-365 exhibits significantly lower emissions, with total H_2O emissions at 161485 kg and NO_x emissions at 17.08 kg. These results underscore the potential of hydrogen-powered aircraft to reduce aviation's environmental footprint. However, the increased H_2O emissions from hydrogen-fueled aircraft, as seen in the significant H_2O emissions in the hydrogen BWB-365 and the hydrogen BWB-162 model, require further exploration due to their potential short-term radiative forcing effects. More details of these emissions impacts can be found in the Appendix.

To assess the climate impacts among the configurations considered here, we assessed the GWP in terms of kg CO_2 equivalent emissions per passenger-kilometer as presented in Fig. 18. This assessment considers GWP values over a 100-year horizon derived from relevant literature. The GWP factors used in our analysis include CO_2 at a factor of 1, HC at 21, CO at 1.7, NOx at 40,

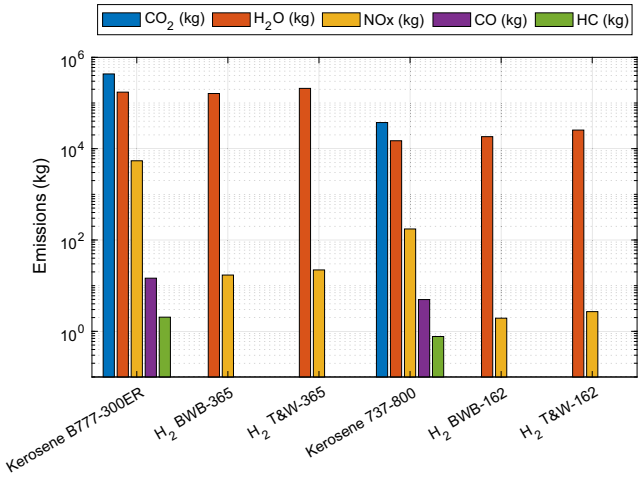

Fig. 17 Comparison of total emissions (CO_2, H_2O, NO_x, CO, HC) for various aircraft models, including conventional (777-300ER, 737-800) and hydrogen-powered configurations (BWB-365, BWB-162, T&W-365, T&W-162).

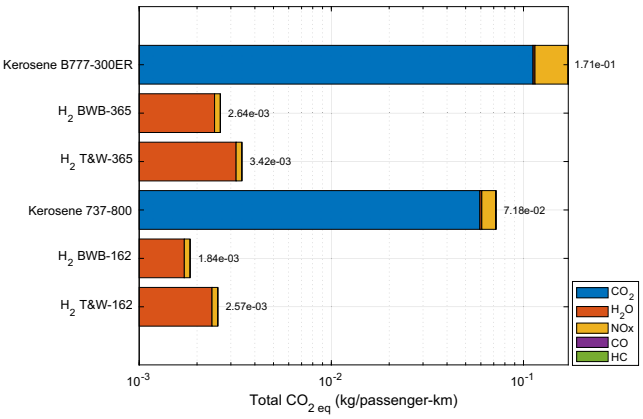

Fig. 18 CO_2 equivalent emissions per PAX-km by aircraft, with 100-year GWP for CO_2, H_2O, NO_x, CO, and HC.

and H_2O at 0.059 [47–49]. This comparative assessment reveals the significant differences in emissions between hydrogen- and kerosene-fueled aircraft. Notably, hydrogen-powered aircraft configurations exhibit substantially lower CO_2 equivalent emissions, particularly in the hydrogen BWB-162 model, with a value of approximately 1.84×10^{-3} kg/passenger · km. In contrast, kerosene-powered models like the Kerosene 737-800 and Kerosene 777-300ER show much higher emissions, with the latter reaching 1.71×10^{-1} kg/passenger · km. It is important to note that 100-year CO_2 equivalent is not the only useful metric for assessing the climate impacts of emissions like water, especially since radiative forcing from water emissions is usually limited to hours. A breakdown of the emission factors and total CO_2 equivalent emissions for various aircraft models can be found in Tables B5 and B6.

IV. Conclusions

Six distinct aircraft configurations are designed and comparatively analyzed within their respective classes. A notable trend of increasing OEW was observed for both the hydrogen-powered BWB-365 and BWB-162, primarily due to the increased wing surface area and cabin planform area. Despite a higher OEW, the hydrogen BWB-365 and BWB-162 exhibited superior fuel efficiency, with a 22.7 and 28.7% lower fuel weight compared to hydrogen T&W-365 and hydrogen T&W-162, respectively. This is mainly attributed to their higher aerodynamic coefficients and the greater energy density of hydrogen fuel. Moreover, the hydrogen-powered BWB-365 achieved a 61% reduction in Megajoule of fuel consumption per passenger-kilometer and a 22% reduction in total takeoff weight per passenger compared to the conventional Boeing 777-300ER. Similarly, the hydrogen BWB-162 showed a 52% decrease and 11% increase compared to the conventional Boeing 737-800, respectively.

Integrating an SOFC/GT powertrain into aircraft necessitates careful consideration of the additional space required for hydrogen fuel tanks. Storing fuel within the wings, as is common in conventional T&W designs, is deemed impractical due to the narrow spaces provided. To maintain the same payload and passenger capacity as T&W aircraft without sacrificing cargo space, extending the fuselage is necessary. However, this extension raises concerns regarding the stress and loading experienced by the aircraft during flight.

The centerbody design of the BWB offers significant potential for scaling the aircraft to accommodate varying payloads. The flat and wide centerbody allows for lateral expansion of the cabin. As demonstrated by Liebeck and the current results, which show that this design can accommodate from 162 to 800 passengers [14]. Nonetheless, challenges exist in ensuring the overall structural integrity of the BWB design and effectively integrating a hydrogen-powered SOFC/GT propulsion system.

Regarding the environmental impacts of hydrogen-powered aircraft, a significant advantage is that the only byproduct of using pure hydrogen as a fuel source is water vapor. Although there are some thermal NOx emissions due to the oxidizer and fuel cell exit flow temperature, the overall impact is considerably lower compared to Jet-A powered aircraft. Notably, NOx emissions for the hydrogen BWB-365 are 99.6% lower than those for a kerosene-powered B777-300ER and 98.9% lower for the hydrogen BWB-162 compared to a conventional B737-800. Moreover, despite that hydrogen fuel aircraft have a higher emissions index per kilogram of fuel, the BWB-365 results in 6% lower H_2O emissions than the B777-300ER, and the BWB-162 is 18% higher than the B737-800.

In conclusion, hydrogen BWB designs show promising advantages in fuel efficiency, significant synergy with hydrogen tanks, and promising scalability. Results indicate a positive trend when scaling down from a 365- to a 162-passenger layout, with weight per passenger reduced by approximately 31.9%. Further research is required to address the structural complexities and integration challenges associated with these innovative propulsion system integrations and configurations. One disadvantage of the SOFC/GT powertrain is the longer startup time required by the SOFC stacks compared to conventional turbojet engines, which may be overcome by significant thermal mass and reasonable amounts of insulation, which were not assessed in the current work. Despite the slow startup time, fuel cell stacks typically have a lower failure rate in terms of electricity production and offer a long operational lifetime. Electrifying the aircraft also allows for distributed propulsion, which provides aerodynamic and environmental advantages. Nevertheless, leveraging the characteristics of BWB designs, hydrogen fuel, and fuel cell technology, while addressing the associated challenges, will enable the aviation industry to progress toward more sustainable and efficient aircraft designs.

Appendix A: Hydrogen Tanks Sensitivity Analysis

Table A1 Sensitivity analysis for the hydrogen storage tanks with various tank efficiencies for hydrogen BWB-365

Wt/Wf	Tank efficiency, %	Total power, MW	TOGW, kg	Weight per PAX, kg
0.23	77	59.9	260887	714
0.33	67	60.9	264068	723
0.43	57	61.6	267233	732
0.53	47	62.3	270475	741
0.63	37	63.1	273796	750

Appendix B: Emission Tables

Table B1 Fuel burnt and emissions by flight segment for example flight trajectory from SFO to HKG aboard a B777-300ER

Segment	Fuel burnt, kg	CO_2, kg	H_2O, kg	NO_x, kg	CO, kg	HC, kg
Taxi	91.316	282.06	112.91	0.50324	3.1575	0.33202
Takeoff	33.966	106.91	42.719	1.7346	0.0042458	0.0010869
Climb	3124.4	9834	3929.8	113.85	0.42804	0.074985
Cruise	1.3158e + 05	4.1416e + 05	1.655e + 05	5263.2	9.2106	1.579
Descent	2397	7543.2	3013	47.94	1.1985	0.043146
Approach	270.89	851.75	340.67	4.3791	0.58511	0.013003
Total	— —	4.3278e + 05	1.7294e + 05	5431.6	14.584	2.0432

Table B2 Fuel burn and emissions by flight segment for example flight trajectory from SFO to HKG aboard a hydrogen BWB-365

Segment	Fuel burn, kg	H_2O emissions, kg	NO_x emissions, kg
Taxi	11.92	107.25	0.01
Takeoff	4.43	39.89	0.00
Climb	407.71	3669.43	0.39
Cruise	17170.54	154534.90	16.35
Descent	312.80	2815.17	0.30
Approach	35.35	318.14	0.03
Total	— —	161484.78	17.08

Table B3 Emissions and fuel burnt for different flight segments for example flight trajectory from SFO to BOS aboard a B737-800

Segment	Fuel burnt, kg	CO_2, kg	H_2O, kg	NO_x, kg	CO, kg	HC, kg
Taxi	15.779	48.964	19.559	0.067848	0.40867	0.048914
Takeoff	6.1638	19.396	7.7498	0.12636	0.0036983	0.00061638
Climb	731.4	2301.6	919.59	12.726	0.3657	0.07314
Cruise	10453	32898	13146	156.8	3.1359	0.52265
Descent	607.28	1909.9	763.17	4.2509	0.91092	0.12146
Approach	43.754	137.5	55.012	0.41566	0.14001	0.0043754
Total	— —	37315	14911	174.38	4.9649	0.77115

Table B4 Fuel burn and emissions by flight segment for example flight trajectory from SFO to BOS aboard a hydrogen BWB-162

Segment	Fuel burn, kg	H_2O emissions, kg	NO_x emissions, kg
Taxi	2.71	24.38	0.00
Takeoff	1.06	9.52	0.00
Climb	125.56	1130.06	0.12
Cruise	1794.50	16150.50	1.71
Descent	104.25	938.28	0.10
Approach	7.51	67.60	0.01
Total	— —	18320.34	1.94

Table B5 Emission factors for different aircraft models

kg/px · km	CO_2	H_2O	NO_x	CO	HC
Kerosene B777-300ER	0.1121	0.044794	0.0014069	3.7774×10^{-6}	5.2922×10^{-7}
H_2 BWB-365	0	0.041827	4.4239×10^{-6}	0	0
Kerosene 737-800	0.059283	0.023689	0.00027704	7.8878×10^{-6}	1.2251×10^{-6}
H_2 BWB-162	0	0.029106	3.0821×10^{-6}	0	0
H_2 T&W-365	0	0.05414	5.7268×10^{-6}	0	0
H_2 T&W-162	0	0.040571	4.2895×10^{-6}	0	0

Table B6 Total CO_2 equivalent emissions for different aircraft models

Aircraft	Total CO_2 eq, kg/ passenger.km
Kerosene B777-300ER	0.17103
H_2 BWB-365	0.0026447
Kerosene 737-800	0.071802
H_2 BWB-162	0.0018405
H_2 T&W-365	0.0034233
H_2 T&W-162	0.0025653

References

[1] Overton, J., "The Growth in Greenhouse Gas Emissions from Commercial Aviation," Issue Brief, Environmental and Energy Study Inst. (EESI), Washington, D.C., 2019, https://www.eesi.org/papers/view/fact-sheet-the-growth-in-greenhousegas-emissions-from-commercialaviation.

[2] Zhu, Y., Fanning, E., Yu, R. C., Zhang, Q., and Froines, J. R., "Aircraft Emissions and Local Air Quality Impacts from Takeoff Activities at a Large International Airport," *Atmospheric Environment*, Vol. 45, No. 36, 2011, pp. 6526–6533. https://doi.org/10.1016/j.atmosenv.2011.08.062

[3] Valencia, E. A., Hidalgo, V., Laskaridis, P., Nalianda, D., Singh, R., and Liu, C., "Design Point Analysis of a Hybrid Fuel Cell Gas Turbine Cycle for Advanced Distributed Propulsion Systems," *51st AIAA/SAE/ASEE Joint Propulsion Conference*, AIAA Paper 2015-3802, , 2015. https://doi.org/10.2514/6.2015-3802

[4] Felder, J., Kim, H., and Brown, G., "Turboelectric Distributed Propulsion Engine Cycle Analysis for Hybrid-Wing-Body Aircraft," *47th AIAA Aerospace Sciences Meeting Including the New Horizons Forum and Aerospace Exposition*, AIAA Paper 2009-1132, 2009. https://doi.org/10.2514/6.2009-1132

[5] Adler, E. J., and Martins, J. R. R. A., "Blended Wing Body Configuration for Hydrogen-Powered Aviation," *Journal of Aircraft*, Vol. 61, No. 3, 2024, pp. 887–901. https://doi.org/10.2514/1.C037582

[6] Chen, Z., Zhang, M., Chen, Y., Sang, W., Tan, Z., Li, D., and Zhang, B., "Assessment on Critical Technologies for Conceptual Design of Blended-Wing-Body Civil Aircraft," *Chinese Journal of Aeronautics*, Vol. 32, No. 8, 2019, pp. 1797–1827. https://doi.org/10.1016/j.cja.2019.06.006

[7] Kimmel, W. M., and Bradley, K. R., A Sizing Methodology for the Conceptual Design of Blended-Wing-Body Transports," NASA, TR NASA CR-2004-213016, Hampton, VA, 2004.

[8] JetZero, "JetZero: The Future Takes Shape," 2023, https://www.jetzero.aero/ [retrieved 22 June 2024].

[9] Norris, G., "Airbus Reveals Refined ZEROe Blended Wing Body Concept," *Aviation Week*, 2022, https://aviationweek.com/shownews/singapore-airshow/airbus-reveals-refined-zeroe-blended-wing-body-concept [retrieved 22 April 2023].

[10] Karpuk, S., Ma, Y., and Elham, A., "Design Investigation of Potential Long-Range Hydrogen Combustion Blended Wing Body Aircraft with Future Technologies," *Aerospace*, Vol. 10, No. 6, 2023, Paper 566. https://doi.org/10.3390/aerospace10060566

[11] Kissoon, S., Mastropierro, F. S., Nalianda, D. K., Rolt, A., and Sethi, B., "Assessment of the BWB Aircraft for Military Transport," *Aircraft Engineering and Aerospace Technology*, Vol. 92, No. 5, 2020, pp. 769–776. https://doi.org/10.1108/AEAT-09-2019-0188

[12] Wells, D. P., Horvath, B. L., and Mccullers, L. A., "The Flight Optimization System Weights Estimation Method," NASA TM-2017-219627, Vol. I, Hampton, VA, 2017

[13] McDonald, R. A., and Gloudemans, J. R., "Open Vehicle Sketch Pad: An Open Source Parametric Geometry and Analysis Tool for Conceptual Aircraft Design," *AIAA Science and Technology Forum and Exposition, AIAA SciTech Forum 2022*, AIAA Paper 2022-0004, 2022. https://doi.org/10.2514/6.2022-0004

[14] Liebeck, R. H., "Design of the Blended Wing Body Subsonic Transport," *Journal of Aircraft*, Vol. 41, No. 1, 2004, pp. 10–25. https://doi.org/10.2514/1.9084

[15] Marchman, J. F., Walz, A., and Grey, K., and Virginia Polytechnic Institute and State University, *University Libraries, Aerodynamics and Aircraft Performance*, Virginia Tech Publishing, Blacksburg, VA, 2018.

[16] Alsamri, K., Rezaei, S., Chung, V., Huynh, J., and Brouwer, J., "Dynamic Modeling of Hydrogen SOFC/GT Powered Aircraft with Integration Analysis," *AIAA SCITECH 2024 Forum*, AIAA Paper 2024-1532, 2024. https://doi.org/10.2514/6.2024-1532

[17] Zhang, B., Maloney, D., Farida Harun, N., Zhou, N., Pezzini, P., Medam, A., Hovsapian, R., Bayham, S., and Tucker, D., "Rapid Load Transition for Integrated Solid Oxide Fuel Cell—Gas Turbine (SOFC-GT) Energy Systems: A Demonstration of the Potential for Grid Response," *Energy Conversion and Management*, Vol. 258, 2022, Paper 115544. https://doi.org/10.1016/j.enconman.2022.115544

[18] McLarty, D. F., "Fuel Cell Gas Turbine Hybrid Design, Control, and Performance," Ph.D. Thesis, Univ. of California, Irvine, 2010, https://www.proquest.com/dissertations-theses/fuel-cell-gas-turbine-hybrid-design-control/docview/758398393/se-2?accountid=14509.

[19] Collins, J. M., and McLarty, D., "All-Electric Commercial Aviation with Solid Oxide Fuel Cell-Gas Turbine-Battery Hybrids," *Applied Energy*, Vol. 265, 2020, Paper 114787. https://doi.org/10.1016/j.apenergy.2020.114787

[20] NASA Glenn Research Center, High Power Density SOFC: Technology Solution Power Generation and Storage," NASA TR NP-2017-07-2426-HQ, NASA Glenn Research Center, Cleveland, OH, 2017.

[21] NASA Technology Transfer Program, "High Power Density Solid Oxide Fuel Cell," NASA Tech Briefs, n.d., https://www.techbriefs.com/component/content/article/tb/pub/briefs/energy/33394.

[22] Scholz, A. E., Michelmann, J., and Hornung, M., "Fuel Cell Hybrid-Electric Aircraft: Design, Operational, and Environmental Impact," *Journal of Aircraft*, Vol. 60, No. 1, 2022, pp. 606–622. https://doi.org/10.2514/1.C036952

[23] Tornabene, R., Wang, X., Steffen, C. J., and Freeh, J. E., "Development of Parametric Mass and Volume Models for an Aerospace SOFC/Gas Turbine Hybrid System," *Proceedings of the ASME Turbo Expo 2005: Power for Land, Sea, and Air, Turbo Expo 2005*, Vol. 5, ASME, 2005, pp. 135–144. https://doi.org/10.1115/GT2005-68334

[24] Felder, J. L., Brown, G. V., DaeKim, H., and Chu, J., "Turboelectric Distributed Propulsion in a Hybrid Wing Body Aircraft," TR ISABE-2011-1340, NASA Glenn Research Center, Cleveland, OH, July 2011.

[25] Asghari, M., "Integration of Solid Oxide Fuel Cell with Liquid Desiccant Cooling for Generation of Combined Cooling and Power for Data Center Application," Ph.D. Dissertation, Dept. of Mechanical and Aerospace Engineering, Univ. of California, Irvine, CA, 2022.

[26] McFarland, C., and Agarwal, R. K., "A Simple Model of Thermal Insulation Design for Cryogenic Liquid Hydrogen Tank, McKelvey School of Engineering, Washington Univ. in St. Louis, April 2022. https://doi.org/10.7936/3ens-v661

[27] Choi, D., Lee, S., and Kim, S., "A Thermodynamic Model for Cryogenic Liquid Hydrogen Fuel Tanks," *Applied Sciences*, Vol. 14, No. 9, 2024, Paper 3786. https://doi.org/10.3390/app14093786

[28] Andersson, G. Z., "Mathematical Modeling and Simulation of Cryogenic Liquid Hydrogen Storage," Master's Thesis, Lund Univ., 2023, http://lup.lub.lu.se/student-papers/record/9116856.

[29] International Civil Aviation Organization, "ICAO Aircraft Engine Emissions Databank," 2023, https://www.easa.europa.eu/en/domains/environment/icao-aircraft-engine-emissions-databank [retrieved 4 June 2024].

[30] Hasanzadeh, A., Chitsaz, A., Mojaver, P., and Ghasemi, A., "Stand-Alone Gas Turbine and Hybrid MCFC and SOFC-Gas Turbine Systems: Comparative Life Cycle Cost, Environmental, and Energy Assessments," *Energy Reports*, Vol. 7, 2021, pp. 4659–4680. https://doi.org/10.1016/j.egyr.2021.07.050

[31] Lundberg, W. L., Israelson, G. A., Moeckel, M. D., Veyo, S. E., Holmes, R. A., Zafred, P. R., King, J. E., and Kothmann, R. E., "A High Efficiency PSOFC/ATS-Gas Turbine Power System," U.S. Dept. of Energy, National Energy Technology Lab., DEAC26-98FT40455, Morgantown, WV, 2001. https://doi.org/10.2172/859228

[32] Sinha, A. A., Srivastava, K., Rajpoot, A. S., Choudhary, T., and Pandey, S., and Sanjay, "A Thermodynamic Approach to Analyze Energy, Exergy, Emission, and Sustainability (3E-S) Performance by Utilizing Low Temperature Waste Heat in SOFC-CHP-TEG System," *International Journal of Hydrogen Energy*, Vol. 63, 2024, pp. 1088–1104. https://doi.org/10.1016/j.ijhydene.2024.03.194

[33] He, Z. J., Chang, C., and Follen, C., "NOx Emissions Performance and Correlation Equations for a Multipoint LDI Injector," *53rd AIAA Aerospace Sciences Meeting*, AIAA Paper 2015-0098, 2015. https://doi.org/10.2514/1.2015-0098

[34] FuelCell Energy, "Solid Oxide Fuel Cell Spec Sheet," 2022, https://go.fuelcellenergy.com/hubfs/Solid%20Oxide%20Fuel%20Cell%20Spec%20Sheet.pdf.

[35] Murphy, D. M., and Koop, T., "Review of the Vapour Pressures of Ice and Supercooled Water for Atmospheric Applications," *Quarterly Journal of the Royal Meteorological Society: A Journal of the Atmospheric Sciences, Applied Meteorology and Physical Oceanography*, Vol. 131, No. 608, 2005, pp. 1539–1565. https://doi.org/10.1256/qj.04.94

[36] Volker, G., Bock, L., Burkhardt, U., Dahlmann, K., Gierens, K., Hüttenhofer, L., Unterstrasser, S., Gangoli Rao, A., Bhat, A., Yin, F., et al., "Assessing the Climate Impact of the AHEAD Multi-Fuel Blended Wing Body," *Meteorologische Zeitschrift*, Vol. 26, No. 6, 2017, pp. 711–725. https://doi.org/10.1127/metz/2016/0758

[37] FlightAware, "FlightAware: CPA881 Flight History from KLAX to VHHH," Dec. 2023, https://www.flightaware.com/live/flight/CPA881/history/20231210/0730Z/KLAX/VHHH [retrieved 22 June 2023].

[38] Jane, F. T., "Jane's All the World's Aircraft," Franklin Watts, 2023.

[39] Page, M., and Vassberg, J., "BWB Enabling Technologis," *33rd ICAS Congress 2022*, 2022, https://www.icas.org/ICAS_ARCHIVE/ICAS2022/data/papers/ICAS2022_0392_paper.pdf.

[40] De Miguel, N., Acosta, B., Moretto, P., and Ortiz Cebolla, R., "The Effect of Defueling Rate on the Temperature Evolution of On-Board Hydrogen Tanks," *International Journal of Hydrogen Energy*, Vol. 40, No. 42, 2015, pp. 14,768–14,774. https://doi.org/10.1016/j.ijhydene.2015.06.038

[41] Rivard, E., Trudeau, M., and Zaghib, K., "Hydrogen Storage for Mobility: A Review," *Materials*, Vol. 12, No. 12, 2019, Paper 1973. https://doi.org/10.3390/ma12121973

[42] Verstraete, D., and Ramsden, K., "Potential of Liquid Hydrogen for Long Range Aircraft Propulsion," Ph.D. Thesis, Cranfield Univ., School of Engineering, Gas Turbine Engineering, 2009, https://books.google.ae/books?id=7MQUyAEACAAJ.

[43] Tiwari, S., Pekris, M. J., and Doherty, J. J., "A Review of Liquid Hydrogen Aircraft and Propulsion Technologies," *International Journal of Hydrogen Energy*, Vol. 57, 2024, pp. 1174–1196. https://doi.org/10.1016/j.ijhydene.2023.12.263

[44] Sharifzadeh, S., Verstraete, D., and Hendrick, P., "Cryogenic Hydrogen Fuel Tanks for Large Hypersonic Cruise Vehicles," *International Journal of Hydrogen Energy*, Vol. 40, No. 37, 2015, pp. 12,798–12,810. https://doi.org/10.1016/j.ijhydene.2015.07.120

[45] Sgueglia, A., Schmollgruber, P., Benard, E., Bartoli, N., and Morlier, J., "Preliminary Sizing of a Medium Range Blended Wing-Body Using a Multidisciplinary Design Analysis Approach," *MATEC Web of Conferences, 8th EASN-CEAS International Workshop on Manufacturing for Growth & Innovation*, Vol. 233, 2018, Paper 00014. https://doi.org/10.1051/matecconf/201823300014

[46] Reist, T. A., and Zingg, D. W., "Aerodynamic Design of Blended Wing-Body and Lifting-Fuselage Aircraft," *34th AIAA Applied Aerodynamics Conference*, AIAA Paper 2016-3874, 2016. https://doi.org/10.2514/6.2016-3874

[47] Fuglestvedt, J., Shine, K., Berntsen, T., Cook, J., Lee, D., Stenke, A., Skeie, R., Velders, G., and Waitz, I., "Transport Impacts on Atmosphere and Climate: Metrics," *Atmospheric Environment*, Vol. 44, No. 37, 2010, pp. 4648–4677. https://doi.org/10.1016/j.atmosenv.2009.04.044

[48] Jungbluth, N., and Meili, C., "Recommendations for Calculation of the Global Warming Potential of Aviation Including the Radiative Forcing Index," *The International Journal of Life Cycle Assessment*, Vol. 24, No. 3, 2019, pp. 404–411. https://doi.org/10.1007/s11367-018-1556-3

[49] Königshofer, B., Boškoski, P., Nusev, G., Koroschetz, M., Hochfellner, M., Schwaiger, M., Juričić, Đ., Hochenauer, C., and Subotić, V., "Performance Assessment and Evaluation of SOC Stacks Designed for Application in a Reversible Operated 150 kW rSOC Power Plant," *Applied Energy*, Vol. 283, 2021, Paper 116372. https://doi.org/10.1016/j.apenergy.2020.116372

J. Vassberg
Associate Editor